

**Jānis Braunfelds**

**DEVELOPMENT OF THE MULTIFUNCTIONAL FIBER  
OPTICAL SENSING SYSTEM AND ITS APPLICATION  
IN MONITORING SOLUTIONS**

Summary of the Doctoral Thesis



**RIGA TECHNICAL UNIVERSITY**  
Faculty of Electronics and Telecommunications  
Institute of Telecommunications

**Jānis Braunfelds**

Doctoral Student of the Study Programme “Telecommunications”

**DEVELOPMENT OF THE MULTIFUNCTIONAL FIBER  
OPTICAL SENSING SYSTEM AND ITS APPLICATION IN  
MONITORING SOLUTIONS**

**Summary of the Doctoral Thesis**

Scientific supervisors:

Professor Dr. sc. ing. VJAČESLAVS BOBROVS

Professor Dr. sc. ing. JURĢIS PORIŅŠ

RTU Press

Riga 2023

Braunfelds, J. Development of the Multifunctional  
Fiber Optical Sensing System and its Application in  
Monitoring Solutions. Summary of the Doctoral Thesis.  
Riga: RTU Press, 2023. – 43 p.

Published in accordance with the decision of  
RTU Promotion Council “P-08” of 23 February 2023, Minutes No.19.

**INDUSTRIĀLAIS  
DOKTORANTS**



**Imt**



Innovation  
Grants for  
Students



Industrial  
Doctor

NATIONAL  
DEVELOPMENT  
PLAN 2020



EUROPEAN UNION  
European Regional  
Development Fund

INVESTING IN YOUR FUTURE

<https://doi.org/10.7250/9789934229220>

ISBN 978-9934-22-922-0 (pdf)

# **DOCTORAL THESIS PROPOSED TO RIGA TECHNICAL UNIVERSITY FOR THE PROMOTION TO THE SCIENTIFIC DEGREE OF DOCTOR OF SCIENCE**

To be granted the scientific degree of Doctor of Science (Ph. D.), the present Doctoral Thesis has been submitted for the defence at the open meeting of RTU Promotion Council on June 2, 2023 at the Faculty of Electronics and Telecommunications of Riga Technical University, 12 Āzenes Street, Room 201.

## **OFFICIAL REVIEWERS**

Dr. sc. ing. Girts Ivanovs

Riga Technical University

Dr. sc. ing. Aleksejs Udalcovs

Ericsson, Sweden

Dr. sc. ing. Kaspars Sudars

Institute of Electronics and Computer Science, Latvia

## **DECLARATION OF ACADEMIC INTEGRITY**

I hereby declare that the Doctoral Thesis submitted for the review to Riga Technical University for the promotion to the scientific degree of Doctor of Science (Ph. D.) is my own. I confirm that this Doctoral Thesis had not been submitted to any other university for the promotion to a scientific degree.

Jānis Braunfelds \_\_\_\_\_.

Date: \_\_.\_\_\_\_.\_\_\_\_.

The Doctoral Thesis has been developed as a set of thematically related scientific publications with a summary in Latvian and English. It has been written in Latvian and consists of an Introduction, 3 chapters, Conclusions, 39 figures, 5 tables, 11 appendices; the total number of pages is 69 (not including appendices). The Bibliography contains 203 titles. The PhD Thesis presents a summary of 10 original scientific articles out of 19 articles published by the author and one patent issued by the Republic of Latvia. Scientific publications have been written in English and are indexed in SCOPUS, IEEE and WoS databases; their total volume is 100 pages. The patent has been written in Latvian; the total volume is 10 pages.

**THE DOCUMENT HAS BEEN SIGNED BY ELECTRONIC SIGNATURE WHICH CONTAINS A  
TIMESTAMP**

## Acknowledgements

I would like to express my gratitude to my scientific supervisors Professor Vjačeslavs Bobrovs and Professor Jurgis Poriņš, as well as Professor Sandis Spolītis, the Head of the Communication Technologies Research Centre of the Institute of Telecommunications of RTU Faculty of Electronics and Telecommunications for their guidance and advice in the course of development of the Thesis.

As a researcher of the Institute of Telecommunications of RTU FET I have had an opportunity to collaborate with many talented and professional colleagues and fellow students. I would like to thank them all for their support, team work, and the knowledge they shared with me. I wish to express my special appreciation to my long-term colleagues Andis Supe, Sandis Spolītis, Uģis Senkāns, Toms Salgals, Armands Ostrovskis, Rihards Mūrnieks and Elvis Haritonovs.

I express my gratitude to *Latvijas Mobilais Telefons*, RTU Design Factory, and the team of Department of Doctoral Studies for their advice, support and efficient collaboration.

Finally, I would like to express the greatest gratitude to my family and friends for their encouragement and faith in me. Your support has been invaluable.

I would like to thank everybody who I have been working with or who has been supporting me but whose names are not mentioned here.

## Table of Contents

<b>General Description of the Thesis</b> .....	7
Topicality of the Theme .....	7
Aim, Tasks and Theses to be Substantiated .....	8
Scientific Novelty and Main Results.....	9
Structure and Volume of the Thesis.....	9
Approbation of Thesis Results and Publications.....	10
<b>Introduction</b> .....	12
<b>Main Results of the Thesis</b> .....	14
<b>1. Determination of the Most Appropriate Parameters of Fiber Bragg Grating for Sensor Network and Long-distance Monitoring Solutions</b> .....	14
<b>2. Interoperability of FOTS and FBG sensor Networks – Assessment of the Impact on the Quality of the Data Transmission Channels</b> .....	19
2.1. Assessment of an Integrated Spectrum-Sliced Optical Fiber Data Transmission and FBG Sensor System.....	19
2.2. Assessment of Interoperability Between Spectrum-Sliced Multichannel Optical Fiber Data Transmission System and FBG Sensor Network .....	21
2.3. FWM Optical Frequency Comb-Based DWDM Optical Data Transmission System with an Integrated FBG Sensor Network.....	23
<b>3. Application of the FBG Optical Sensors in Road Structural Health Monitoring</b> .....	26
3.1. Road SHM by Using FBG Optical Sensor Embedded in the Road Pavement Surface Layers .....	27
3.2. Road SHM by Using FBG Sensor Embedded into the Cement-treated RAP Mixture Layer of the Road Pavement.....	31
<b>Conclusions</b> .....	35
<b>References</b> .....	36

## List of Abbreviations

<b>AADT</b>	Annual Average Daily Traffic	<b>MUX</b>	Multiplexer
<b>AADTT</b>	Annual Average Daily Truck Traffic	<b>MZM</b>	Mach-Zehnder Modulator
<b>AC</b>	Asphalt Concrete	<b>NRZ</b>	Non-Return to Zero
<b>APD</b>	Avalanche Photodiode	<b>OBLS</b>	Optical Broadband Light Source
<b>ASE</b>	Amplified Spontaneous Emission	<b>OBPF</b>	Optical Band Pass Filter
<b>AWG</b>	Arbitrary Waveform Generator	<b>OC</b>	Optical Circulator
<b>BER</b>	Bit-Error Rate	<b>ODN</b>	Optical Distribution Network
<b>BOTDA</b>	Brillouin Optical Time Domain Analyzer	<b>OFC</b>	Optical Frequency Comb
<b>BOTDR</b>	Brillouin Optical Time Domain Reflectometry	<b>OLT</b>	Optical Line Terminal
<b>BTB</b>	Back-to-Back	<b>ONU</b>	Optical Network Unit
<b>CDM</b>	Code-division Multiplex	<b>OPC</b>	Optical Power Coupler
<b>CW</b>	Continuous Wave	<b>OPS</b>	Optical Power Splitter
<b>DCM</b>	Dispersion Compensating Module	<b>OS</b>	Optical Switch
<b>DEMUX</b>	Demultiplexer	<b>OSA</b>	Optical Spectrum Analyzer
<b>DSO</b>	Digital Storage Oscilloscope	<b>OTDR</b>	Optical Time Domain Reflectometer
<b>DSP</b>	Digital Signal Processing	<b>PC</b>	Power Coupler
<b>DWDM</b>	Dense Wavelength Division Multiplexing	<b>PD</b>	Photodiode
<b>EAM</b>	Electro-Absorption Modulator	<b>PM</b>	Power Meter
<b>EDFA</b>	Erbium Doped Fiber Amplifier	<b>PON</b>	Passive Optical Network
		<b>RAP</b>	Reclaimed Asphalt Pavement
<b>EF</b>	Electrical Filter	<b>SBS</b>	Stimulated Brillouin Scattering
<b>FBG</b>	Fiber Bragg Grating	<b>SHM</b>	Structural Health Monitoring
<b>FEC</b>	Forward Error Correction	<b>SLED</b>	Superluminescent Diode
<b>FWD</b>	Falling Weight Deflectometer	<b>SLS</b>	Side-Lobe Suppression
<b>FWHM</b>	Full Width Half Maximum	<b>SMA</b>	Stone Mastic Asphalt
<b>FWM</b>	Four Wave Mixing	<b>SMF</b>	Single Mode Fiber
<b>GI-FMF</b>	Graded-Index Few Mode Fiber	<b>SOA</b>	Semiconductor Optical Amplifier
<b>HNLF</b>	High Non-Linearity Fiber	<b>SS-WDM</b>	Spectrum Sliced WDM
<b>IEEE</b>	Institute of Electrical and Electronics Engineers	<b>VOA</b>	Variable Optical Attenuator
<b>ITU-T</b>	International Telecommunication Unit-Telecommunication Standardization Sector	<b>WDM</b>	Wavelength Division Multiplexing
		<b>WIM</b>	Weigh in Motion

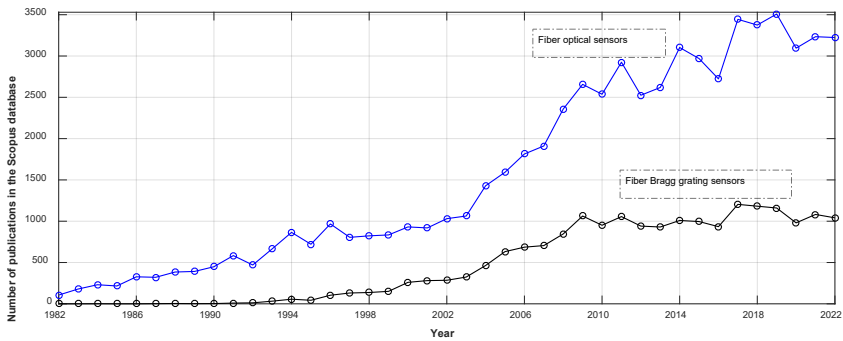
# GENERAL DESCRIPTION OF THE THESIS

## Topicality of the Theme

The number of sites and territories in Latvia and across the world that need different kinds of real-time health monitoring (roads, barrages, bridges, pipelines, dams, railways, buildings and other structures) is constantly growing. Over the last decade, monitoring of various processes and sites, as well as sensor-based safety control of the public infrastructure, has been playing an increasingly important role [1]–[3]. Since monitoring often should be conducted at long distances across many locations simultaneously, in corrosive environments under electromagnetic interference or in environments without power supply, FBG can be applied in such types of monitoring [4]–[10].

Nowadays, the infrastructure of optical networks has not been exploited and utilized in its full capacity. The author sees high potential in the extension of the infrastructure applications using optical fiber sensors. Taking into consideration that the infrastructure of optical networks is located at/near roads, bridges, tunnels, railways, dams, etc., it can be used as a transmission medium for monitoring these objects of infrastructure. “Dark” optical fiber lines can be applied in such monitoring solutions, or working lines can be used, utilizing their free frequency ranges. To promote further development of such solutions, it is important to develop high value optical FBG sensor networks for long distance monitoring (40+ km) solutions, to provide interoperability of communication and sensor solutions and to ensure integration of high-quality sensors in various infrastructure objects (e.g., road pavement) for monitoring purposes.

In order to better understand the topicality of the present theme, the analysis of research articles available in SCOPUS database was conducted. The articles were searched using such parameters as the title, key words, and abstracts containing the key words “optical fiber sensors” and “fiber Bragg grating sensors”. In the last decade, on average, 3130 research articles with keywords “optical fiber sensors” were published, whereas there were 1052 articles containing key words “fiber Bragg grating sensors”. The detailed dynamics by year is shown in the figure below. The high number of available research articles, the growing dynamics of the characteristic curve, and high citation rate of the author’s research articles [9], [11] demonstrate that the research topic has been and will remain topical and will ultimately promote development of technology.



Number of scientific articles in SCOPUS database by year.

### **Aim, Tasks and Theses to be Substantiated**

**The aim of the Thesis** is to integrate a fiber optical Bragg grating sensor network in optical fiber communication systems and to evaluate application of FBG sensors in real-time road monitoring solutions.

**The following tasks were defined to achieve the aim of the Thesis:**

1. To analyze the types, main parameters, and principles of operation of optical sensors and to evaluate opportunities of their integration in the existing optical network infrastructure and their application.
2. To determine the most relevant parameters for optical FBG sensor networks and long-distance monitoring solutions using a mathematical modelling software.
3. To integrate FBG sensor networks in optical data transmission systems experimentally as well as inside the mathematical modelling environment and to evaluate their compatibility.
4. To install optical FBG strain and temperature sensors (in the upper, binder, and cement-treated reclaimed layers of the road pavement) inside the layers of a used road pavement.
5. To experimentally assess real-time measurements of the traffic induced strain loads on the different layers of road pavement.

**Thesis statements to be defended:**

1. In order to develop an FBG sensor network solution for at least 40 km long distance remote monitoring operations, signal reflectivity of at least 90 % must be ensured at SLS > 20 dB and FWHM < 0.2 nm
2. It is possible to develop a hybrid optical system based on a single broadband light source that consists of 10 Gbit/s 32-channel SS-WDM PON and five optical FBG sensors network while ensuring the necessary quality of the received signal over a 20 km long transmission line.

3. FBG optical temperature and strain sensors can be integrated in the cement-treated reclaimed asphalt pavement mixture layer for structural health monitoring applications and real-time measurements of the traffic induced strain data.

### **Scientific Novelty and Main Results**

1. A mathematical model of a 40 FBG sensor network that ensures monitoring over the distance of at least 40 km has been developed.
2. A single broadband light source-based 32-channel 10 Gbit/s dense spectrum-sliced optical fiber data transmission system with an integrated 5 FBG sensor network solution has been developed.
3. A technological solution for integration of optical FBG sensors in the road surface, binder and cement-treated reclaimed asphalt pavement mixture layers has been developed to measure temperature and traffic load induced strains in real-time.
4. The technique of FBG strain sensor calibration has been developed to carry out assessment of traffic load induced strain data.

**The results achieved in the course of Thesis development have been applied in the following projects:**

1. ERDF project “RTU Innovation Grants for Students”, participant of RTU and LMT Industrial Doctor Programme, 1.1.1.3/18/A/001, 1 July 2019 – 31 July 2022.
2. RTU research project “Fiber optical FBG sensors for structural health monitoring of road pavement”, B4223, 2 January 2020 – 31 December 2020 (scientific project manager).
3. ERDF PIP “Passive fiber optical sensors for energy efficient health monitoring of transport infrastructure” 1.1.1.1/16/A/072, 1 March 2017 – 1 March 2020.
4. RTU research project “Development of a combined energy efficient fiber optical data transmission and sensing system”, B4000, 7 January 2019 – 6 January 2020.
5. RTU research project “Development of a multi-functional fiber optical sensing system”, B3472, 15 January 2018 – 31 December 2018.

### **Structure and Volume of the Thesis**

The Thesis has been developed as a thematically related collection of scientific publications dedicated to the research on fiber optical FBG sensors in mathematical modelling and their integration in fiber optical data transmission system and application in real-time monitoring of road pavement. The Thesis summarizes the information presented in 5 original scientific journal publications, 4 scientific conference proceedings (indexed in Scopus, IEEE and Web of Science), one monograph and one patent issued by the Republic of Latvia.

## Approbation of Thesis Results and Publications

The main results of the Thesis have been published in 5 original scientific articles, one monograph, and one patent of the Republic of Latvia. The research results have been presented at 4 scientific conferences (indexed in Scopus, IEEE and Web of Science).

### Scientific publications in journals

1. **J. Braunfelds**, U. Senkans, P. Skels, R. Janeliukstis, J. Porins, S. Spolitis, V. Bobrovs, Road Pavement Structural Health Monitoring by Embedded Fiber Bragg Grating Based Optical Sensors, *Sensors*, 2022, pp. 1–13. DOI: 10.3390/s22124581.
2. **J. Braunfelds**, E. Haritonovs, U. Senkans, I. Murans, J. Porins, S. Spolitis, Designing of Fiber Bragg Gratings for Long-distance Optical Fiber Sensing Networks. Modelling and Simulation in Engineering, pp. 1–13, 2022. DOI: 10.1155/2022/8331485.
3. **J. Braunfelds**, U. Senkans, P. Skels, R. Janeliukstis, T. Salgals, D. Redka, I. Lyashuk, J. Porins, S. Spolitis, V. Haritonovs, V. Bobrovs, FBG-Based Sensing for Structural Health Monitoring of Road Infrastructure (2021) *Journal of Sensors*, 2021, art. no. 8850368. DOI: 10.1155/2021/8850368.
4. **J. Braunfelds**, K. Zvirbule, U. Senkans, R. Murnieks, I. Lyashuk, S. Spolitis and V. Bobrovs, Application of FWM-based OFC for DWDM Optical Communication System with Embedded FBG Sensor Network, *Latvian Journal of Physics and Technical Sciences*, p.14. 2021 (in Press).
5. U. Senkans, **J. Braunfelds**, I. Lyashuk, J. Porins, S. Spolitis, V. Bobrovs, Research on FBG-Based Sensor Networks and Their Coexistence with Fiber Optical Transmission Systems (2019) *Journal of Sensors*, 2019, art. no. 6459387. DOI: 10.1155/2019/6459387.

### Scientific monographs

1. **J. Braunfelds**, S. Spolitis, J. Porins, V. Bobrovs, Fiber Bragg Grating Sensors Integration in Fiber Optical Systems, *IntechOpen*, 2020, DOI: 10.5772/intechopen.94289.

### The results of the Thesis presented in the proceedings of scientific conferences (indexed in Scopus, IEEE, Web of Science)

1. **J. Braunfelds**, U. Senkans, P. Skels, I. Murans, J. Porins, S. Spolitis, V. Bobrovs, Fiber Bragg Grating Optical Sensors for Road Infrastructure Monitoring Applications, (2022) *Optics InfoBase Conference Papers, Applied Industrial Optics*, pp. 1–2, DOI: 10.1364/AIO.2022.W1A.2.
2. **J. Braunfelds**, U. Senkans, I. Lyashuk, J. Porins, S. Spolitis and V. Bobrovs, Unified Multi-channel Spectrum-sliced WDM-PON Transmission System with Embedded FBG Sensors Network, 2019 *Photonics & Electromagnetics Research Symposium – Spring (PIERS-Spring)*, 2019, pp. 3327–3333, DOI: 10.1109/PIERS-Spring46901.2019.9017809.
3. U. Senkans, **J. Braunfelds**, I. Lyashuk, J. Porins, S. Spolitis, V. Haritonovs, V. Bobrovs, FBG sensors network embedded in spectrum-sliced WDM-PON transmission system operating on single shared broadband light source, (2019) 2019 *Photonics and Electromagnetics Research Symposium – Fall, PIERS – Fall 2019 – Proceedings*, art. no. 9021628, pp. 1632–1639. DOI: 10.1109/PIERS-Fall48861.2019.9021628.

4. U. Senkans, **J. Braunfelds**, S. Spolitis, V. Bobrovs, Research of FBG Optical Sensors Network and Precise Peak Detection (2018) Proceedings – 2018 Advances in Wireless and Optical Communications, RTUWO 2018, art. no. 8587859, pp. 139–143. DOI: 10.1109/RTUWO.2018.8587859.

**The results of the Thesis presented at scientific conferences (not indexed in Scopus, IEEE, Web of Science)**

1. U. Senkans, **J. Braunfelds**, P. Skels, J. Porins, S. Spolitis, V. Bobrovs, Fiber Bragg Grating Sensors for Hybrid WDM-PON systems and structural health monitoring of road infrastructure, First Workshop for ERI on Telecommunication and Networks, March 14–15, 2022.
2. **J. Braunfelds**, U. Senkans, J. Porins, S. Spolitis, V. Bobrovs, Fiber Bragg Grating Sensors for structural health monitoring of road infrastructure. First Workshop of EU+ Sustainability Lab (2021).
3. **J. Braunfelds**, J. Porins, S. Spolitis, V. Bobrovs, FBG sensors for structural health monitoring of road infrastructure. Quantum Optics and Photonics (2021).
4. E. Haritonovs, S. Spolitis, **J. Braunfelds**, Evaluation of fiber Bragg grating applications in optical sensor solutions, 63rd International scientific conference of RTU, Riga, Latvia, 2022.
5. **J. Braunfelds**, U. Senkans, I. Murans, J. Porins, S. Spolitis, V. Bobrovs, Application of FBG optical sensors in road pavement SHM, 63rd International scientific conference of RTU, 2022.
6. I. Zalitis, **J. Braunfelds**, S. Spolitis, FBG sensor networks and their integration in fiber optical communication systems, 63rd International scientific conference of RTU, 2022.
7. U. Senkans, **J. Braunfelds**, S. Spolitis, V. Bobrovs, Multi-channel SS-WDM-PON transmission system with embedded FBG sensors network, 60th International scientific conference of RTU, Riga, Latvia, October 15, 2019.
8. A. Ostrovskis, **J. Braunfelds**, Research and evaluation of fiber optical sensors in FOTS solutions, 60th International scientific conference of RTU, Riga, Latvia, October 15, 2019.
9. **J. Braunfelds**, V. Bobrovs, Development and Evaluation of Fiber Optical Sensors System, 59th International scientific conference of RTU, Riga, Latvia, October 12, 2018.
10. U. Senkans, **J. Braunfelds**, S. Spolitis, V. Bobrovs, Research of FBG Optical Sensors Network and Effective Detection of Channel Spacing, 59th International scientific conference of RTU, 2018.
11. E. Haritonovs, **J. Braunfelds**, S. Spolitis, Evaluation of Fiber Bragg Grating Characteristic Parameters for Optical Sensors Solutions, RTU 62nd Student Conference of Applied Science (2021).
12. A. Ostrovskis, **J. Braunfelds**, Research and Evaluation of Fiber Optical Sensors in FOTS Solutions, RTU 60th Student Conference of Applied Science (2019).
13. A. Nikulins, **J. Braunfelds**, Research and Evaluation of Optical Intensity Sensors, RTU 60th Student Conference of Applied Science (2019).

## INTRODUCTION

Nowadays, the majority of the population understands the meaning of the term “optical internet”. Optical fiber used as a medium for transmission of information is used in order to provide a service to the customers. Along with the development of technology, the number of applications of such optical fibers is increasing, and fiber optic sensors are among these solutions.

Application of optical fibers in sensor designs was reported already in 1970. It became possible due to the invention of the laser in 1960 and development of low attenuation optical fibers in 1966 [12]. In the early 1990s, optical sensors, which could measure temperature, strain, pressure and other parameters, were put into use. In turn, the beginning of the 21st century was characterized by wide application of optical sensors, which measured temperature over the entire fiber length, which allowed oil and gas companies to monitor their networks and timely repair damages. In building construction sector, optical fiber sensors were used to monitor critical areas of the buildings and to plan timely repair works. In the meantime, process efficiency has been considered as an issue of growing importance, and optical fiber sensors start playing an ever-increasing role.

A lot of progress has been made since, and today optical fiber sensors allow measuring changes in a wide range of parameters, such as strain, pressure, temperature, movement, vibration, acceleration, rotation, moisture level, humidity, amperage, chemical composition, and many other parameters [12]. Development of those sensors was to a great extent promoted by the advantages optical fibers have over other kinds of sensors, for example, high sensitivity, immunity against electromagnetic interference, passive sensors, lightweight and compact size, chemical resistance, multiplexing opportunities, suitability for long-distance change monitoring, low-level induced attenuation [12], wide range of measured chemical and physical parameters [13]–[16].

Optical fiber sensors are classified into 2 large groups: intrinsic and extrinsic optical fiber sensors.

**In the case of extrinsic optical fiber sensors**, optical signals are propagated outside the optical fiber and they need a sensing element at the end of the fiber. Materials that change their optical parameters, for instance, refraction index, absorption, fluorescence, reflection, etc., allow producing a wide range of sensors depending on a parameter to be monitored. Nowadays, extrinsic optical fiber sensors still play an important role in the general range of optical fiber sensors. Basically, extrinsic optical fiber sensors use dual fiber connector sensors and Fabry–Pérot interferometers [17].

**Intrinsic optical fiber sensors** use optical fiber as a sensing element. Intrinsic optical fiber sensors are classified into macrobending and microbending sensors, fiber Bragg grating sensors (FBG), as well as Rayleigh, Raman, and Brillouin scattering based sensors. In the case of optical fiber scattering sensors (Rayleigh, Raman, and Brillouin), optical fiber is used both as a transmission medium and as a sensitive component. In sensors of such kind, optical fiber works as a sensor over the whole length.

The discovery of fiber Bragg grating significantly promoted the development of the optical fiber sensor and telecommunications industry. Fiber Bragg grating is produced by modifying the refractive index within the core of an optical fiber (along the longitudinal axis). FBG has a wide range of applications, for example, in dispersion compensation, optical filters, optical fiber amplifiers, lasers, multiplexors, demultiplexers, sensors, and other solutions [18]. The reflected Bragg wavelength is sensitive to various physical parameters, for this reason, FBG can be used as an optical sensor in order to monitor and determine changes of physical parameters over time. FBG are quasi-distributed sensors allowing for simple multiplexing – using them in sensor network solutions (typically, approximately 100 sensors, but using CDM-WDM allows achieving the array of up to 1000 sensors) [19]. The spatial resolution of FBG sensors is equal to the grating length (typically, 2–10 mm, in rare cases reaching up to 20 mm). Sampling frequency for standard optical sensors signal interrogation unit is up to 1 kHz, in rare cases it reaches 5 kHz. FBG sensors can be used in various industries to measure and monitor temperature, strain, movement, pressure, vibration, and other physical parameters. FBG sensors tend to be most commonly used (2/3 of cases) in structural health monitoring (e.g., bridges, dams, roads, buildings, pipelines, etc.) [20]–[22].

Most commonly, optical FBG sensors are used for strain and temperature measurement in monitoring of various roads [11], [23], [24], railways [25]–[27], buildings [28]–[30], composite materials [31]–[34], and health care facilities [35]–[37].

FBG temperature sensors are used to compensate for temperature changes for FBG (strain, movement, vibration, pressure, etc.) sensors, as well as in monitoring of temperature [38]–[39] and structural health monitoring (SHM) [40]–[42].

FBG vibration sensors are used mainly in the oil and gas industry [43], [44], SHM [45], [46], as well as in 2D and 3D vibration monitoring solutions [43], [47], [48].

In turn, FBG pressure sensors are used in pipeline [49], [50], tank [51], and borehole [42] monitoring. Research results relatively often report on different developed pressure (including, 2D and 3D) sensors [52]–[54] used for monitoring purposes.

FBG movement sensors are classified by the range into micromovement ( $l = 0 - 10 \text{ mm}$ ) and movement ( $l > 10 \text{ mm}$ ) sensors. Micromovement sensors are less common, they are used in monitoring of structure [55]–[57] and soil [58] movement. In turn, movement sensors are used in industrial [59]–[60], railway [61]–[62] and health care [50] solutions, as well as in monitoring of building structures [57], [63], [64] and ground movement [65], [66].

## Main Results of the Thesis

The research conducted in the course of the doctoral studies was aimed at finding the most appropriate fiber Bragg grating parameters for sensor networks and long-distance monitoring solutions, assessing integrability of various optical data transmission systems and their interoperability with FBG sensor solutions, as well as applicability of these sensors for real-time monitoring of road infrastructure.

### 1. DETERMINATION OF THE MOST APPROPRIATE PARAMETERS OF FIBER BRAGG GRATING FOR SENSOR NETWORK AND LONG-DISTANCE MONITORING SOLUTIONS

The majority of optical FBG sensors available in the market has low side-lobe suppression (SLS) (typically,  $SLS < 15\text{dB}$  [67], [68]) and/or low reflectivity (typically, 7–40 % [67], [69]), and occupy a wide spectral band ( $FWHM > 0.3\text{ nm}$  [68]), which does not allow for efficient use of these sensors for long-distance monitoring purposes (at least 40 km) and their application in sensor networks.

The research articles [70] and [71] report on the research wherein mathematical simulation software was used in modelling FBG gratings for sensor network solutions. The research in [70] has achieved the most appropriate grating parameters in terms of bandwidth (0.13 nm) and SLS (34 dB), but with reflectivity of just 53 %. In turn, the research in [71] has achieved the most appropriate grating parameters in terms of reflectivity (99.9 %) and SLS (95.6 dB), but with high FWHM of 0.434 nm.

To allow for using sensors in remote monitoring at long distances and in sensor network solutions, they should meet the following parameters:

- maximally high reflectivity ( $>90\%$ );
- the narrowest possible bandwidth of a reflected signal ( $FWHM < 0.2\text{ nm}$ );
- maximally high SLS value ( $SLS > 20\text{ dB}$ ).

FBG sensors with the given parameters (reflectivity  $>90\%$  and  $FWHM < 0.2\text{ nm}$ ) can be designed using traditional uniform gratings [71]–[72]. To ensure FBG sensor SLS of at least 20 dB, it is necessary to use grating apodization. Meeting the requirements of all three parameters towards FBG sensors is ensured through adaptation of grating length, longitudinal modifications of grating refraction index ( $\Delta n$ ), and apodization shape. In the course of research, the mathematical simulation software “OptiGrating” [73]–[74] was used to develop gratings in SMF, their reflection spectrum range was measured, the data were processed in MATLAB environment and grating reflectivity curves, FWHM and SLS dependence on grating length (interval from 1–20 mm) at uniform, sine, raised sine and Gaussian grating apodization (at  $\Delta n = 0,5 \times 10^{-4}$ ;  $1 \times 10^{-4}$ ;  $1,5 \times 10^{-4}$ ;  $2 \times 10^{-4}$ )

were plotted. The fiber core had a grating integrated with the following longitudinal modifications of the refractive index:

$$\text{Gaussian apodization} \quad \Delta n(x) = \Delta n \cdot \exp \exp \left\{ -\ln \ln(2) \cdot \left( \frac{2 \cdot \left( x - \frac{L}{2} \right)}{s \cdot L} \right)^2 \right\}; \quad (1.1)$$

$$\text{sine apodization} \quad \Delta n(x) = \Delta n \cdot \sin \left( \frac{\pi \cdot x}{L} \right); \quad (1.2)$$

$$\text{raised sine apodization:} \quad \Delta n(x) = \Delta n \cdot \sin^2 \left( \frac{\pi \cdot x}{L} \right), \quad (1.3)$$

where  $L$  is grating length,  $\Delta n$  is modification of the grating refractive index,  $s$  is taper length = 0.5, and  $x$  is the coordinate of light that is propagation along the length of the grating ( $0 \leq x \leq L$ ).

As shown in Fig. 1.1, grating reflectivity grows along with the increase of the grating length. Higher reflectivity is ensured by the uniform FBG followed by FBG with sine apodization. As it can be seen in Fig. 1.2, the uniform FBG demonstrates the lowest SLS values, which do not reach the minimal threshold SLS value of the grating. For this reason such FBG may not be considered most appropriate for sensor network and long-distance monitoring solutions. Higher SLS values (33–38 dB) ensure FBG with the Gaussian apodization at grating length 1–7 mm, but within 9–20 mm range, higher SLS is ensured by the raised sine apodization (30–32 dB).

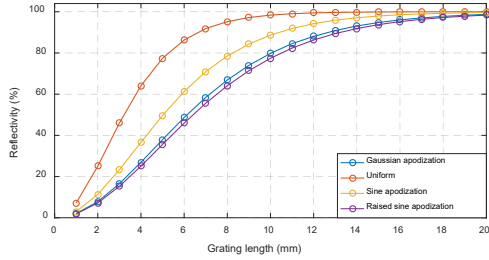


Fig. 1.1. Comparison of FBG reflectivity at  $\Delta n = 1.5 \times 10^{-4}$  for uniform FBG and FBG with the Gaussian, sine, and raised sine apodization.

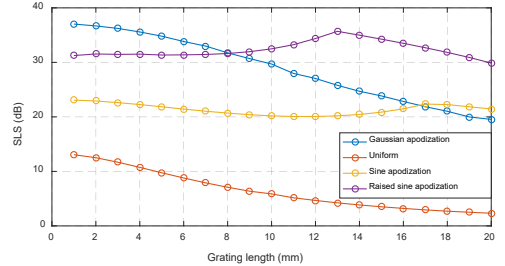


Fig. 1.2. Comparison of FBG SLS at  $\Delta n = 1.5 \times 10^{-4}$  for uniform FBG and FBG with the Gaussian, sine, and raised sine apodization.

The results (Fig. 1.3) show that FBG with grating lengths from 1 to 6 mm are not the best option for sensor networks because they occupy a broad spectral band. Taking into account that any sensor signal processing and analyzing device has a limited transmitter-broadband light source and receiver-spectrometer bandwidth, the use of FBG with a narrower spectral band allows positioning a greater number of sensors on one fiber. Within the narrowest band grating length interval of 1–7 mm, uniform FBG are used followed by the sine and Gaussian apodization. Within the grating length range of 8–20 mm, the narrowest band can be reached using FBG with the Gaussian apodization followed by sine apodization.

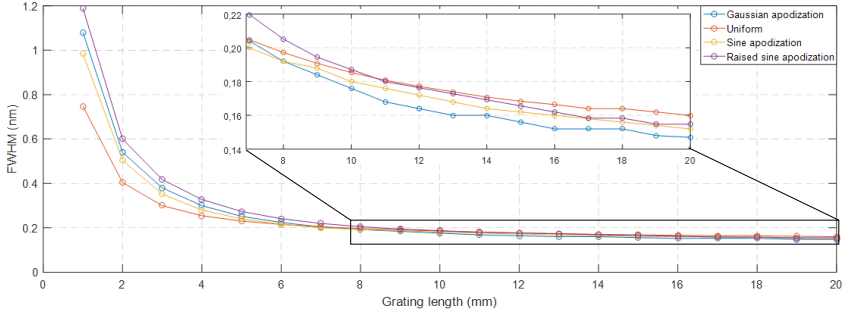


Fig. 1.3. Comparison of FBG FWHM at  $\Delta n = 1.5 \times 10^{-4}$  for uniform FBG and FBG with the Gaussian, sine, and raised sine apodization.

Table 1 summarizes the most appropriate FBG grating and apodization parameters for FBG sensor networks and long-distance monitoring solutions. The table does not reflect the uniform FBG because it does not ensure the minimum SLS requirement. As we can see from the Table 1 data, the raised sine apodization provides relatively similar reflectivity and FWHM as does Gaussian apodization, but SLS values are significantly better for raised sine apodization than they can be observed from Gaussian apodization. Based on the research data, the raised sine apodization is the most appropriate option for sensor networks and long-distance monitoring solutions because such type of apodization can help achieve comparatively high parameters for FBG gratings at the applied  $\Delta n$ . The length of the grating can be reduced when applying higher modulation indexes. However, a higher modulation index increases the spectral band and thus the FWHM value of an FBG.

Table 1.1

FBG grating parameters for FBG with the raised sine, Gaussian and sine apodization at  $\Delta n$  values  $1 \times 10^{-4}$ ,  $1.5 \times 10^{-4}$  and  $2 \times 10^{-4}$

Apodization type	$\Delta n (\times 10^{-4})$	Grating length (mm)	Reflectivity (%)	FWHM (nm)	SLS (dB)
Raised sine	1.0	20	90.3	0.112	35.6
	1.5	13	90.0	0.173	35.7
	2.0	10	90.4	0.228	35.4
Gaussian	1.0	19	90.0	0.110	26.0
	1.5	14	93.1	0.160	24.7
	2.0	10	91.7	0.216	26.9
Sine	1.0	16	90.9	0.118	20.1
	1.5	11	91.9	0.176	20.7
	2.0	13	99.0	0.210	22.5

The relatively best FBG results (reflectivity = 90.3 %, FWHM = 0.112 nm, and SLS = 35.6 dB) are observed for raised sine apodization with a modulation index  $1 \times 10^{-4}$  and grating length of 20 mm. The sensor network with 40 FBG sensors in the wavelength band of 1530 to 1569 nm (spacing between the sensors is 1 nm) is developed based on these FBG parameters to validate the found optimal parameters. The reflected optical signal spectrum is shown in Fig. 1.4.

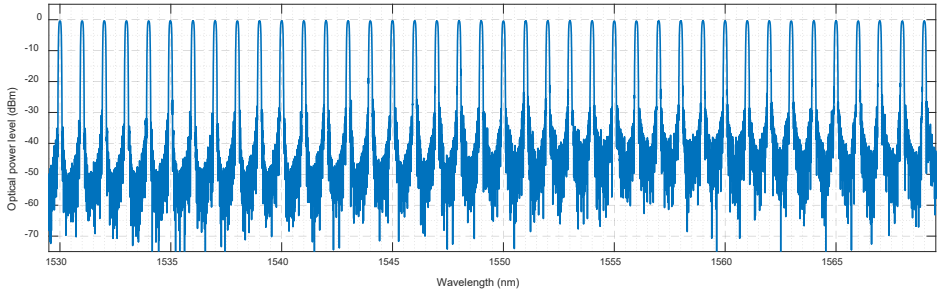


Fig. 1.4. The reflected spectrum for FBG-based sensor network with the raised sine apodization at  $\Delta n = 1 \times 10^{-4}$  and grating length of 20 mm.

The sensor network (Fig. 1.4) with 40 sensors is characterized by high reflectivity (>90 %) and SLS value (~30 dB). Sensor's network SLS value decreased ~5 dB due to side lobes overlapping.

For testing of FBG operation distance, we have, firstly, developed an additional simulation setup (see Fig. 1.5) by using VPIphotonics mathematical modelling software. The developed simulation model was validated in the laboratory environment against commercial FBG sensor network. The FBG sensor transmission characteristic curve for FBG sensors was integrated in the simulation model. An optical spectrum analyzer and signal processing device were used as a receiving part of the model to measure the signal spectrum BTB, at 20 km, 40 km, and 60 km transmission distances.

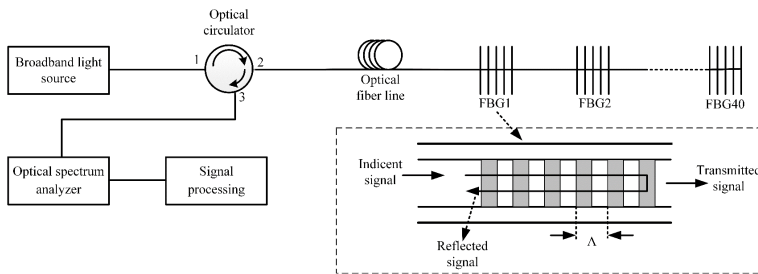


Fig. 1.5. Simulation setup for testing FBG sensor operation distance.

Figure 1.6 demonstrates that at SMF length of 60 km it is possible to determine central wavelengths and SLS value fluctuates from 9 to 11 dB. This means that the FBG sensor network

with the raised sine apodization at  $\Delta n = 1 \times 10^{-4}$  and grating length of 20 mm can be used in long-distance (>60 km) monitoring solutions.

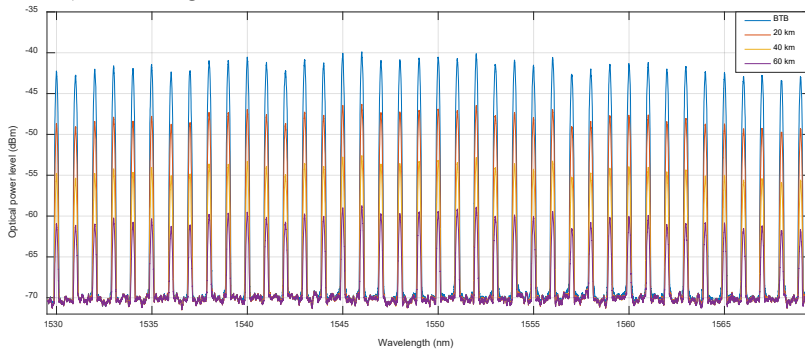


Fig. 1.6. Reflected optical signal spectrum after BTB, 20 km, 40 km, and 60 km transmission.

**Summary:** The achieved results allow concluding that the set requirements (reflectivity > 90 %; FWHM < 0.2 nm; SLS > 20 dB) for the functioning of FBG sensor network monitoring solutions at least over the distance of 40 km can be met with raised sine, Gaussian, and sine apodization. The most appropriate results (reflectivity = 90.3 %, FWHM = 0.112 nm, SLS = 35.6 dB) were demonstrated by FBG with the raised sine apodization at  $\Delta n = 1 \times 10^{-4}$  and  $L = 20$  mm, which allow using FBG sensor networks in long-distance (60+ km) monitoring solutions.

The original article on the research reflected upon in this section is attached (**Annex I**) to the Thesis.

## 2. INTEROPERABILITY OF FOTS AND FBG SENSOR NETWORKS – ASSESSMENT OF THE IMPACT ON THE QUALITY OF THE DATA TRANSMISSION CHANNELS

Along with the development of information and communication technology and growing daily user demands, more and more new and upgraded solutions and systems are being developed. Taking into account favorable installation of optical networks and low utilization rate, as well as advantages of optical sensors and a wide range of their applications, it is necessary to assess the opportunities offered by sensor integration in the optical network infrastructure. In order to assess future opportunities of integrating FBG sensors in fiber optical data transmission systems it is necessary to assess their interoperability and conduct impact analysis.

One of the most attractive ideas associated with optical sensor networks and data transmission systems is to design their inputs based on a single broadband light source. In this case, spectrally sliced wavelength division multiplexing (SS-WDM) technology is used for data transmission. The main advantages of this technology are described in the research article [75], for instance, cost-effectiveness and simplification of the transmitting side.

### 2.1. Assessment of an Integrated Spectrum-Sliced Optical Fiber Data Transmission and FBG Sensor System

A single shared broadband light source-based FOTS with integrated FBG sensors was tested using mathematical simulations and laboratory experiments. The system setup is presented in Fig. 2.1. It consists of the transmitter side, optical distribution network, and receiver side.

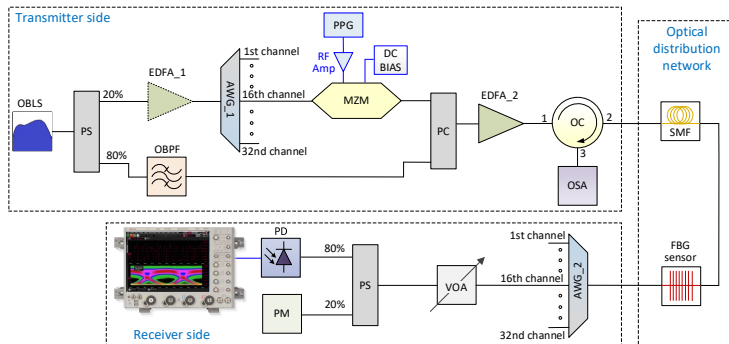


Fig. 2.1. Spectrum-sliced WDM fiber optical transmission system with embedded FBG sensing system fed by a single shared broadband light source.

Assessment of data transmission quality using the mathematical simulation software was performed for a 1.5 Gbit/s spectrum-sliced fiber optical data transmission system with/without an

integrated FBG sensor (see Fig. 2.2). The results show that power penalty of the integrated optical data transmission and sensing system (with and without FBG sensor) at FEC threshold  $2.3 \times 10^{-3}$  for back-to-back (BTB) transmission is 0.5 dB, whereas for transmission over 20 km long SMF fiber it reaches 0.2 dB. In turn, power penalty for the integrated optical data transmission and sensing system (with sensors) at FEC threshold of  $2.3 \times 10^{-3}$  (compared to BTB and 20 km long fiber) is 0.7 dB.

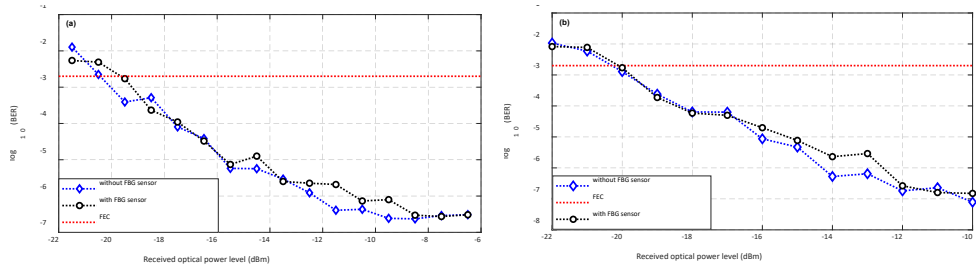


Fig. 2.2. BER versus average received optical power of 1.5 Gbit/s spectrum-sliced data signals for (a) B2B transmission and (b) after transmission over 20 km long SMF fiber.

The results of data transmission quality assessment experimentally implemented for SS-WDM optical fiber data transmission and sensing system with FBG are presented in the eye diagram in Fig. 2.3 and BER correlation graph in Fig. 2.4.

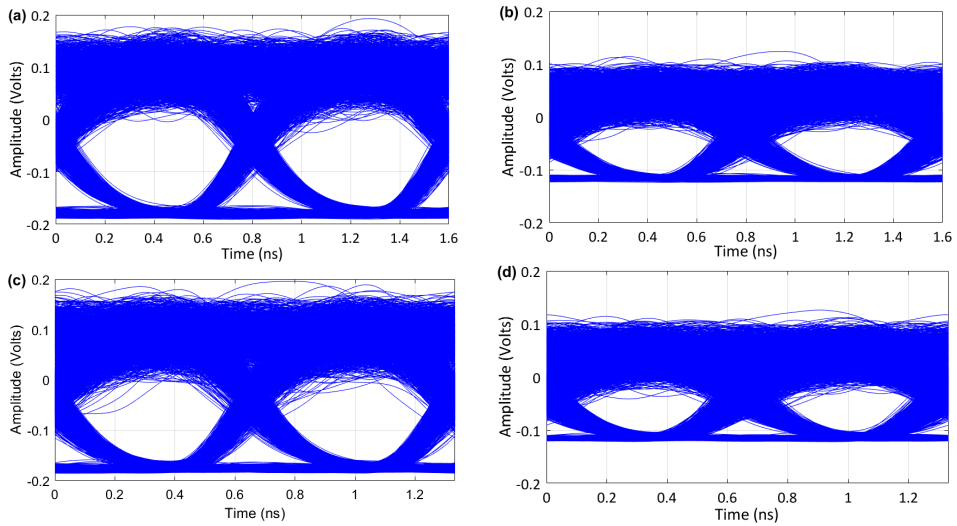


Fig. 2.3. Eye diagrams of received SS-WDM FOTS: (a) 1.25 Gbit/s B2B signal; (b) 1.25 Gbit/s signal after 20 km transmission; (c) 1.5 Gbit/s B2B signal; (d) 1.5 Gbit/s signal after 20 km transmission.

As shown in Fig. 2.3 (a) and (b), at data transmission rate of 1.25 Gbit/s, the eye diagram for BTB case looks widely open and BER is equal to  $4.6 \times 10^{-16}$ , but after transmission over 20 km

BER value decreases and is equal to  $1.3 \times 10^{-9}$ . In turn, at the transmission rate of 1.5 Gbit/s,  $BER = 9.7 \times 10^{-12}$  for BTB transmission (Fig. 2.3 (c)), but after 20 km transmission (Fig. 2.3 (d)), it is  $6.1 \times 10^{-7}$ .

The results presented in Fig. 2.4 demonstrate that power penalty of spectrum-sliced optical fiber 1.5 Gbit/s data transmission and sensing system, comparing BTB transmission and transmission over 20 km at FEC threshold ( $BER = 2.3 \times 10^{-3}$ ), is 1.5 dB. Such power loss is observed mainly due to dispersion and noise of a broadband ASE light source. Increasing data transmission rate from 1.25 to 1.5 Gbit/s, data transmission quality deteriorates and BER values decrease.

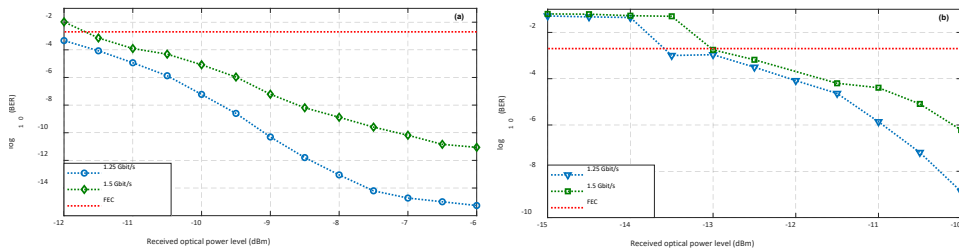


Fig. 2.4. BER versus average received optical power of 1.25 Gbit/s and 1.5 Gbit/s SS-WDM FOTS signals for (a) B2B transmission and (b) after transmission over 20 km long SMF span.

The achieved results demonstrate that a common broadband light source can be used for spectrum-sliced optical fiber data transmission and FBG sensing systems and that they are compatible, it is also possible to carry out error-free data transmission over 20 km long SMF transmission line at 1.25 and 1.5 Gbit/s data transmission rates.

## 2.2. Assessment of Interoperability Between Spectrum-Sliced Multichannel Optical Fiber Data Transmission System and FBG Sensor Network

Interoperability between a 32-channel 10 Gbit/s spectrum-sliced wavelength dense passive optical network (SS-WDM PON) and an FBG sensing network was assessed with a mathematical simulation software RSOFT OptSim, the simulation model is presented in Fig. 2.5.

The simulation model setup is based on the setup given in Fig. 2.1 making the following improvements:

- a semiconductor optical amplifier (SOA) was used to depress ASE intensity fluctuations;
- a Mach-Zehnder modulator (MZM) was replaced with an electric absorption modulator (EAM) immune to signal polarization state;
- PDs were replaced with avalanche photodiodes (APD) that can function at lower signal power levels.

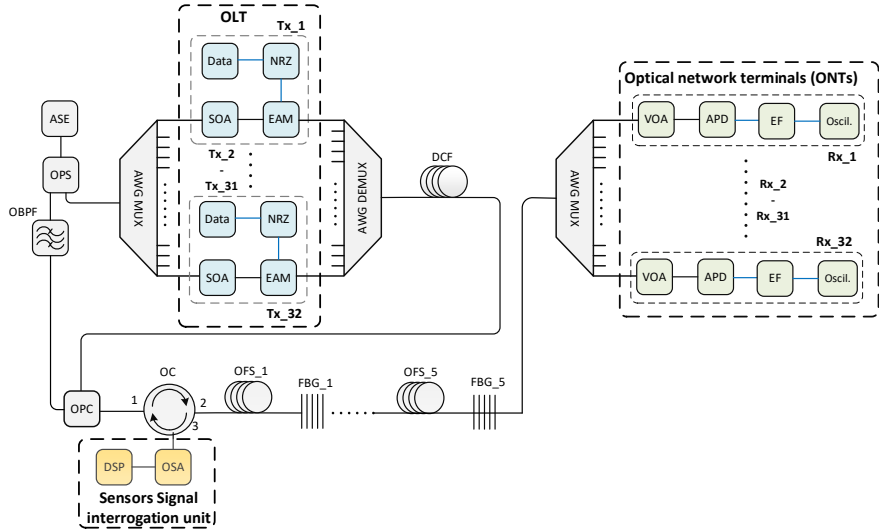


Fig. 2.5. Simulation model of a spectrum-sliced 32-channel FOTS with an integrated FBG sensor network.

These improvements ensure operation of the system over the distance of 20 km using a 32-channel 10 Gbit/s SS-WDM PON with an integrated 5 FBG sensor network. Analyzing efficient interoperability, the impact of sensors on the quality of the transmitted signal was assessed. The impact can be evaluated by comparing the signal quality of a data channel system with a system with the integrated data and sensor channels. To compare the systems, a BER correlation graph was plotted (see Fig. 2.6).

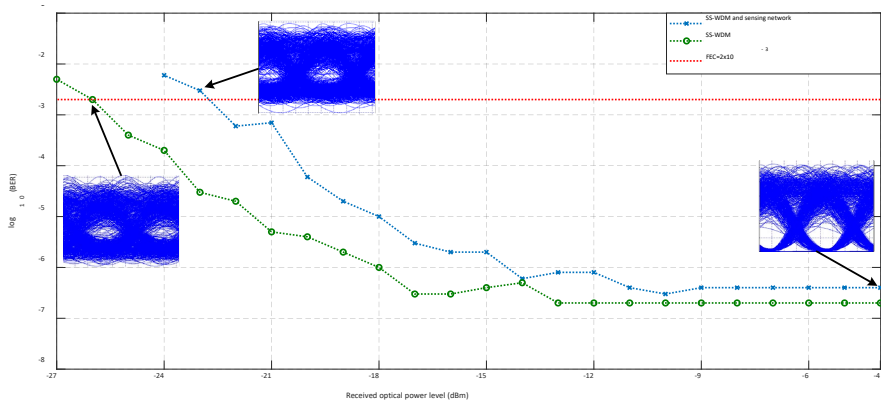


Fig. 2.6. Assessment of BER correlation versus received signal power for a spectrum-sliced 32-channel optical data transmission system with an integrated FBG sensor network at SMF length of 20 km.

The mathematical simulation model assumes a 7% reserve for the data transmission rate (simulations were carried out at 10.7 Gbit/s) to allow for the use of the forward error correction (FEC) code. In this case, the acceptable BER threshold is  $2 \times 10^{-3}$ , which means that the data transmission system can function efficiently at such a value. The measured BER value for SS-WDM PON data channels and FBG sensor network is  $4 \times 10^{-7}$ , but for the system based on data channels it is  $2 \times 10^{-7}$ . The power penalty was calculated based on the measurement results, it is equal to 3.25 dB (comparing the results of an SS-WDM-PON data channel with and without FBG sensor network at BER threshold value of  $2 \times 10^{-3}$ ).

### 2.3. FWM Optical Frequency Comb-Based DWDM Optical Data Transmission System with an Integrated FBG Sensor Network

Mathematical simulation model was conducted to develop and evaluate the performance of a four-wave mixing-based optical frequency comb (FWM-OFC) 8-channel DWDM transmission system with an integrated FBG sensor network. The mathematical simulation model developed using RSOFT OptSim consists of an optical line terminal (OLT), optical distribution network (ODN), and optical network units (ONUs) (see Fig. 2.7).

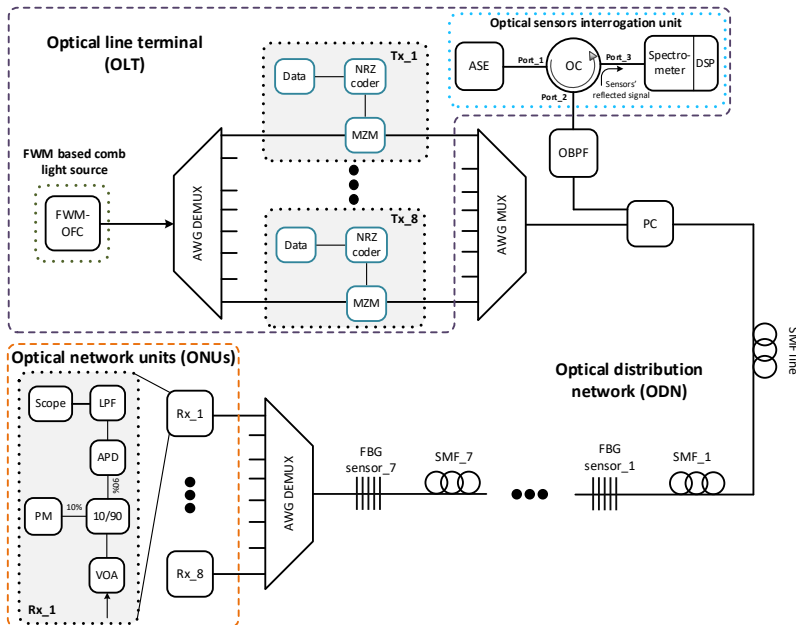


Fig. 2.7. Mathematical simulation model for the 8-channel DWDM-PON system based on FWM OFC with the integrated sensor network of 7 temperature sensors.

FWM-OFC was generated using two continuous wave (CW) lasers, an optical power coupler, high nonlinearity fiber (HNLf); an OSA was used for comb determination. The CW laser output power (20 dBm) and HNLf length (2 km) were set to achieve the frequency comb with the maximum number of combs and high flat amplitude at the output. CW lasers central frequencies were set at 193.1 and 193.15 THz to ensure that their inter-channel spacing was 50 GHz (according to recommendations of ITU-T G.694.1 [76]). The OFC-generated FWM frequency comb had an average power level of 0 dBm, fluctuation was below 3 dB, and 33 dB sideband suppression was in 192.9–193.25 THz frequency range.

The parameters of a commercial [77] FBG sensor experimentally in lab measured conditions were integrated in the mathematical simulation model: transmitted and reflected spectrum and technical parameters (central wavelength, FWHM, reflectivity, etc.).

VOA in ONUs units, 10/90 % power splitter, power meter was used to measure BER correlation graphs (Fig. 2.9.) and monitor the input power in APD photodiode (sensitivity  $-20$  dBm at  $BER \leq 10^{-12}$ ). A  $-3$  dB 7.5 GHz Basel low pass filter (LPF) was used to filter noises.

The fourth channel demonstrating the lowest performance was used in evaluation of data transmission quality. Figure 2.8 shows the oscilloscope’s graph of the received signal change over time for NRZ signal of an integrated 10 Gbit/s system after transmission over 50 km through the SMF fiber. As observed in Figs. 2.8 and 2.10 (b), NRZ signal has the evident dispersion effect, which results in propagation of the pulses.

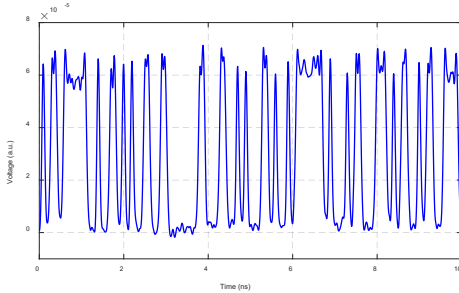


Fig. 2.8. The received signal graph for a 10 Gbit/s NRZ signal after 50 km long transmission.

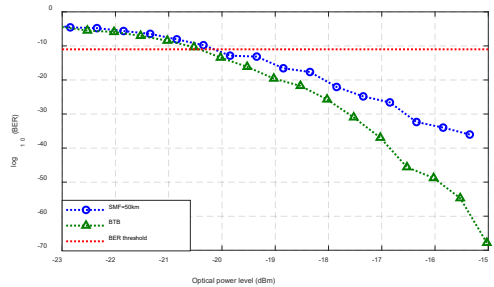


Fig. 2.9. BER versus the received signal power for an 8-channel FOTS with an integrated FBG sensor network.

The system model under study featuring an integrated optical sensor and dense WDM-PON systems, must have a BER of at least  $<10^{-12}$ , normally considered as BER threshold for error-free transmission [78]–[80]. Eye diagram for the integrated system after BTB transmission and transmission over 50 km are presented in Fig. 2.10. Eye diagram is widely open, which allows for error-free transmission. BER of the BTB configuration is equal to  $8 \times 10^{-67}$ , but after transmission over 50 km it is  $9.4 \times 10^{-37}$ .

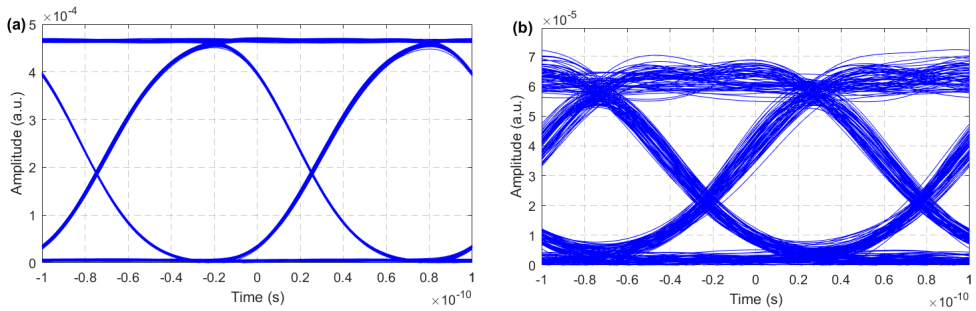


Fig. 2.10. Eye diagram for the data channel with the worst-performance in the combined system after (a) BTB and (b) 50 km long transmission.

**Conclusion:** The research and results show that FBG sensors can be integrated in DWDM, SS-WDM optical fiber data transmission system without any significant impact on the quality of data transmission. BER for data channels of the hybrid single-broadband light source-based system built with 32-channel 10 Gbit/s SS-WDM PON and a FBG sensor network is  $4 \times 10^{-7}$ , but for the system without a FBG network it is  $2 \times 10^{-7}$ .

The original scientific publications and the patent of the Republic of Latvia referring to the research discussed above are attached in **Annexes II-VIII** to the Thesis.

### 3. APPLICATION OF THE FBG OPTICAL SENSORS IN ROAD STRUCTURAL HEALTH MONITORING

To ensure high safety of civil infrastructure, such as roads and bridges, assessment of structural integrity in relation to the load-carrying capacity, which decreases due to aging, deterioration, or damage, must be carried out continuously. The asphalt concrete pavement deteriorates under the increasing traffic and complex climate conditions, i.e., with changing temperature and humidity depending on seasonality [81]. FBG sensors fit perfectly for instant real-time identification of structural deformation, fatigue, load-carrying capacity, cracking, and construction defects in road structures [11], [23], [82]–[87]. Since measurements often must be carried out in rural areas or in the environments exposed to electromagnetic fields, or the environments with no power supply, the use of optical fiber sensors is constantly growing.

An 8-channel optical sensor signal processing interrogation unit and optical distribution network were used for structural health monitoring (see Fig. 3.1). In this technical solution, the optical sensor signal processing interrogation unit functions as a transceiver, with the transmitting part based on SLED broadband source (FWHM = 55 nm), in turn, an optical spectrometer and a DSP block are the receiving part. Compared to OSA, the optical spectrometer ensures  $10^3$  times faster ( $OSA\ 5\ \frac{\text{reads}}{\text{sec}}$  [88], spectrometer  $5000\ \frac{\text{reads}}{\text{sec}}$ ) performance, which is very essential for accurate assessment of strains caused by vehicle loads in motion. The digital signal processor (DSP) receives the spectrometer data, detects central frequencies of the sensor(s) and calculates temperature and strain values. The OS is used to ensure switching from one port to another at a pre-set time interval. The OS allows parallel real-time monitoring of 8 different channels (sensors, sensing network). The optical sensor signal processing interrogation unit is connected to SMF cable and FBG temperature and strain sensors embedded in the road pavement.

The location for FBG sensor integration into pavement structure was chosen in accordance with the recommendation given in European Weigh-In-Motion. Roads A2 (Riga–Sigulda–Estonian border) and A8 (Riga–Jelgava–Lithuanian border) were selected for the research.

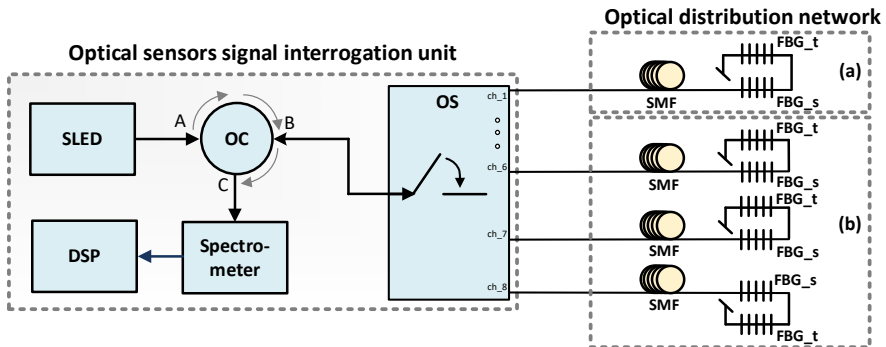


Fig. 3.1. System setup for strain and temperature monitoring.

### 3.1. Road SHM by Using FBG Optical Sensor Embedded in the Road Pavement Surface Layers

Commercial FBG strain [89] and temperature [90] sensors integration in road pavement (see Fig. 3.2) was carried out in 2019–2020 in 2 locations within the framework of the reconstruction project of Road A2 (37 km, Riga direction).

A commercial surface mounted FBG strain sensor (grating length 10 mm) was integrated into glass/epoxy composite patches (250 mm × 15 mm) [89] and FBG temperature sensor [90] – into a ceramic tube (diameter 3 mm, length 23 mm). The temperature sensor was integrated into the ceramic tube to isolate the sensor from strain impacts.

In location (a) 57°07'18.4"N 24°40'02.6"E, FBG strain and temperature sensors were embedded in the road pavement between the layers of 30 mm stone mastic asphalt (SMA11) and 60 mm asphalt concrete (AC11). The sensors were embedded at the depth of 25 mm. In location (a), the road pavement has a multilayer structure (30 mm SMA11, 60 mm AC11, 150 mm rubble, sand), but in location (b) – one-layer structure (70 mm AC11 and gravel). In location (b) 57°07'07.4"N 24°39'04.1"E, FBG strain and temperature sensors were embedded in the 70 mm asphalt concrete (AC11) layer of the temporary road at the depth of 25 mm.



Fig. 3.2. Embedded FBG sensors on the carriageway in locations (a) and (b).

Taking into account that the strain caused by traffic depends not only on the load, but also on the road pavement temperature, it is essential to develop an FBG sensor calibration technique. A falling weight deflectometer (FWD) is used in FBG sensor calibration (see Fig. 3.3), which provides a fixed calibrated load to the FBG sensor. Falling weight deflectometers are in widely

used for nondestructive pavement testing and are used as a research or structural evaluation method [91]–[93]. Measured FWD load pulse over time at 50 kN load is presented in Fig. 3.4.



Fig. 3.3. FWD equipment.

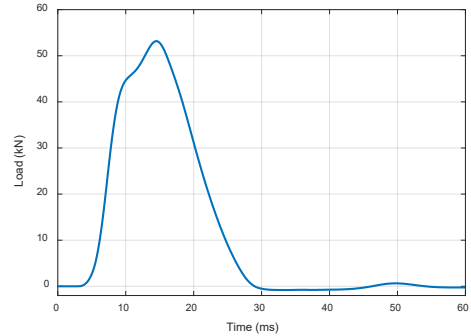


Fig. 3.4. Measured load pulse that is induced by the FWD.

An FWD device was used to assess the operating distance of the FBG sensor in the horizontal direction. The research was done in location (a). The FWD device load plate center was placed at 4 distances (precisely on the sensor and at the distance of 300mm, 600mm, and 900 mm), which applies a fixed  $48.9 \pm 0.5$  kN load drops 6 times (see Table 3.1). During all measurements, temperature was compensated using an FBG sensor. As it can be seen in Table 3.1, results gathered with the FBG sensors show the possibility to precisely (the relative scatter 4.8–12.8 %) detect the strain values, which allows to evaluate the real operation of the pavement structure under load. As it can be seen, the highest strain value (averaging  $151.8 \pm 9.9$   $\mu\text{m}/\text{m}$ ) is detected when the center of the FWD load plate is located over the embedded FBG strain sensor.

Table 3.1

FBG sensor measured strain ( $\mu\text{m}/\text{m}$ ) values depending on horizontal distance between the FWD plate center and the sensor

No. of FWD drop	Horizontal distance of the FWD plate with respect to the FBG sensor (mm)			
	0	300	600	900
1	162.5	91.5	24.6	12.5
2	145.9	77.6	27.0	13.1
3	142.7	80.5	24.2	12.2
4	149.5	73.4	28.3	12.1
5	161.6	85.8	25.7	13.2
6	148.5	71.2	25.1	13.2
Average value of measured strain ( $\mu\text{m}/\text{m}$ )	$151.8 \pm 9.9$	$80.0 \pm 10.2$	$25.8 \pm 2.1$	$12.7 \pm 0.6$

FBG strain sensors are fixed to the asphalt side, then monitoring with high accuracy can be realized from the side where the sensor is embedded. This is the main disadvantage of this method, which must be taken into consideration when applying the integration process of the sensors. For

fixed one-way traffic, it does not create monitoring restrictions, but if the traffic direction is changing, then it is necessary to integrate FBG sensors on both sides.

The FWD equipment measured the drop's load after each drop with its sensors. It was observed that in full measurement, the spread of the load in all cases was less than 1 %. The measurements were taken in summer at the road pavement layer temperature of 20.5 °C.

In order to evaluate the impact of the road pavement temperature on the measured strain, another session of measurements, therefore, was repeated in autumn (pavement temperature 6.9 °C). The comparison of the results at 6.9 °C and 20.5 °C is given in Fig. 3.5. During the experiment, the FWD load of drops was  $51.98 \pm 0.94$  kN. In order to evaluate the impact of the road pavement temperature on the measured strain, another session of measurements was repeated in autumn. As can also be seen, all values of the measured strain were lower in autumn compared to those in summer. The same tendency was observed in research [84]. The strain values were higher in warmer weather because of the stiffness that decreases at higher temperatures; so, as a result, strain values are increasing. Therefore, it is very important to take into consideration the temperature of the road when carrying out the second part of our research – strain measurements from passing vehicles.

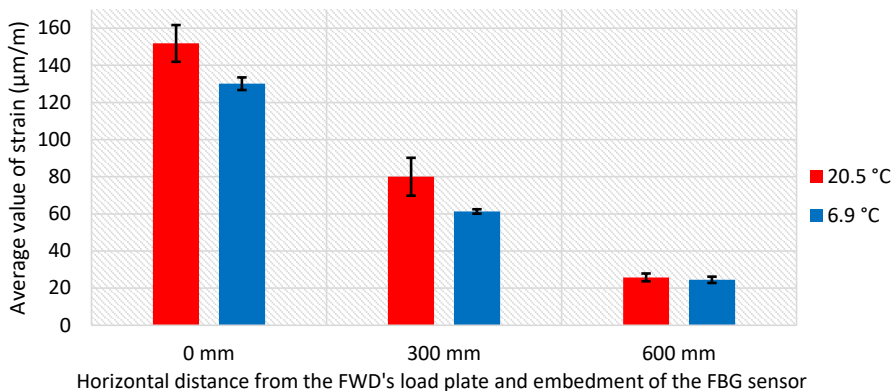


Fig. 3.5. Average value of strain for FWD drops when road temperature is 6.9 °C and 20.5 °C.

Real-time monitoring of vehicle traffic was realized in September 2019 on the temporary road section in location (b). The average temperature of the road pavement layer (measured by an FBG temperature sensor) during the measurements was +25.2 °C. Parallel to the real-time strain measurements, a video was taken in order to be certain that the road traffic changes are calibrated with the strain measurements, as well as to see the “strain-pattern” of different vehicles, mainly trucks. It can be seen that the truck traffic in particular is generating the highest strain in the pavement structure. If the graph is zoomed in, then the number of vehicle axis and the strain value of each vehicle axis can be detected. From the measured FBG strain, sensor data shows that the “G” truck’s last axis (5) creates the highest strain or relative deformation value, which is

375.6  $\mu\text{m/m}$ . The second highest strain value (356.4  $\mu\text{m/m}$ ) was created by the “B” gravel truck that has 3 axes. It is important to note that in Fig. 3.6, upper part visually does not show all of the trucks that were passing by, for example, at the time spans of 73, 728, 891, 986, and 1084 s. Measured strain values are comparable and similar to those shown in research [94].

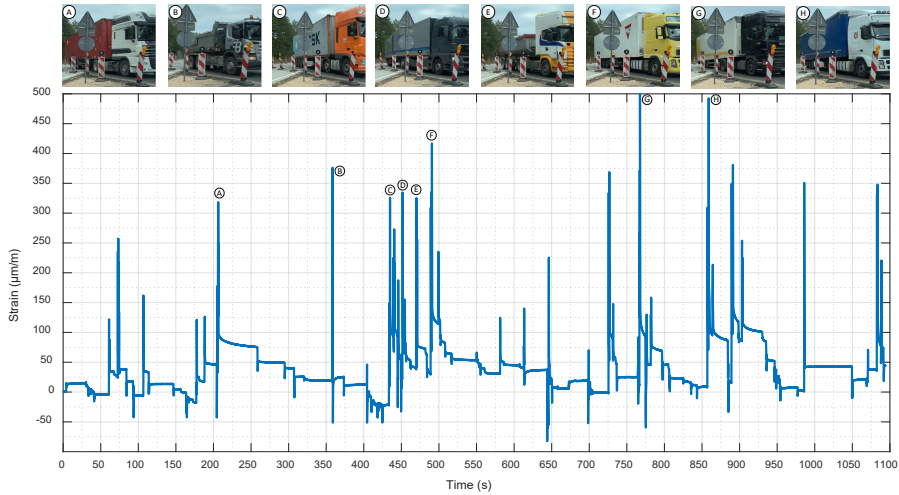


Fig. 3.6. Measured real-time strain graph of passing traffic by the embedded FBG sensor.

The summary of the measurements gathered by the road truck traffic while using FBG sensors is shown in Fig. 3.7. Here, a focus is made on the road’s truck traffic, not the traffic of the passenger cars, as trucks cause the highest applied strain values and damage to the road pavement. The graph represents the generated truck strain value histogram. It is important to add that the strain value histogram contains all the measurement data, not only those presented in Fig. 3.6.

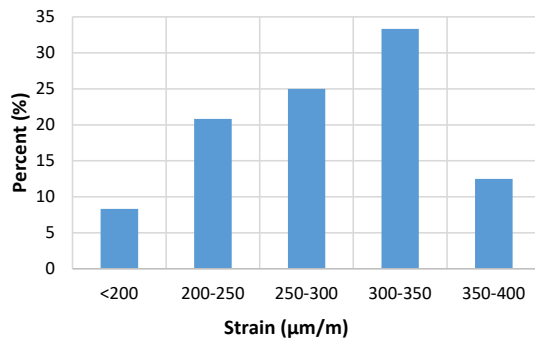


Fig. 3.7. Histogram of strain values generated by trucks measured with embedded FBG sensors.

As it can be seen in the histogram (Fig. 3.7), trucks most often (33 % of the time) can be put into the category that generates strain of 300–350  $\mu\text{m}/\text{m}$ . If all of the data is collected and compared, then trucks, on average, generate 282  $\mu\text{m}/\text{m}$  strain value each.

### 3.2. Road SHM by Using FBG Sensor Embedded into the Cement-treated RAP Mixture Layer of the Road Pavement

In 2020–2021, FBG sensors were embedded in the cement-treated reclaimed asphalt pavement (RAP) mixture layer of Meitene–Jelgava–Riga highway (A8) surfacing ([geographical location](#)). A commercial embedded-type strain sensors [95] with the range of  $\pm 5000 \mu\epsilon$ , tolerance  $< 1 \mu\text{m}$ , central wavelength of 1544.8 nm, and a temperature sensor [96] with operation range from  $-40 \text{ }^\circ\text{C}$  to  $120 \text{ }^\circ\text{C}$ , accuracy  $\pm 0.3 \text{ }^\circ\text{C}$  and central wavelength of 1554.558 nm were installed. The sensors were embedded into the cement-treated RAP mixture layer of the road surfacing at 25 mm depth (total depth of embedment is 240 mm), see Fig. 3.8.

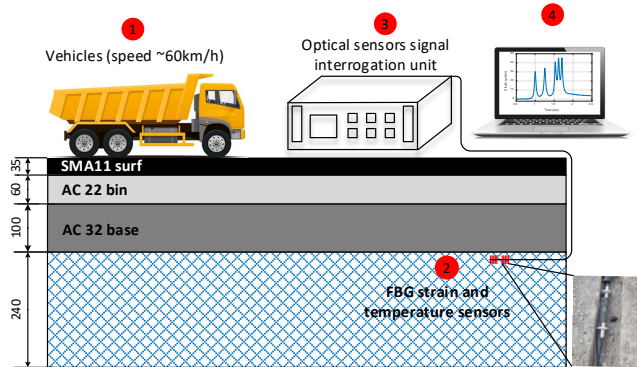


Fig. 3.8. Schematic setup of the FBG optical sensors' embedment (mm) and placement for strain and temperature measurement experiments.

As seen in Fig. 3.9, when generating strain with an FWD deflectometer (load of 50 kN) precisely above an FBG sensor, average strain  $\Delta\epsilon_{\text{avg}}$  is 34.63  $\mu\text{m}/\text{m}$ , but in the scenario with the load plate 50 cm away from the sensor, average strain is 14.03  $\mu\text{m}/\text{m}$ . The measurements were taken at the cement-treated RAP mixture layer temperature 1–1.5  $^\circ\text{C}$ . The correlation between the strain and distance can be characterized with a linear function.

The results show that during the research it is essential to ensure that vehicles drive onto the sensor, or as close to the sensor as possible. In cases when it is not possible to fulfil the above requirement, the author recommends applying sensor networks in order to place sensors in a parallel circuit at some offset distance (e.g., 20 cm).

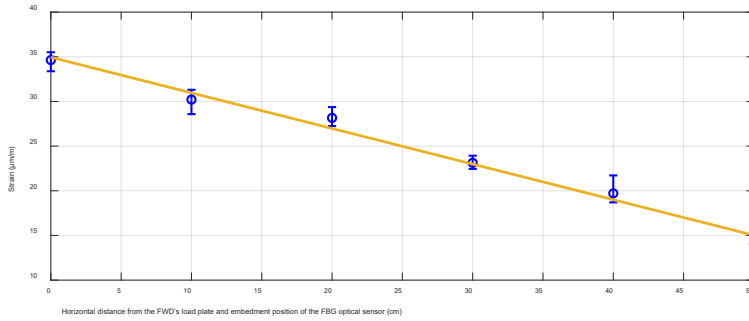


Fig. 3.9. Correlation between the received strain values and FWD's load plate centrum position.

Figure 3.10 demonstrates the correlation of the FBG sensor measured average strain values and FWD generated stress in the case when sensors are embedded in the cement-treated RAP mixture layer of road A8 surfacing. During the measurements, the cement-treated RAP mixture layer temperature was 1–1.5 °C. Along with an increase of FWD generated stress (in the range of 470–1170 kPa with a step of 200 kPa), the strain values show linear growth. The achieved characteristic curve data allow for sensor calibration in the real environment. Such technique of sensor calibration should be used to weigh in motion solutions to determine strain values versus vehicle mass.

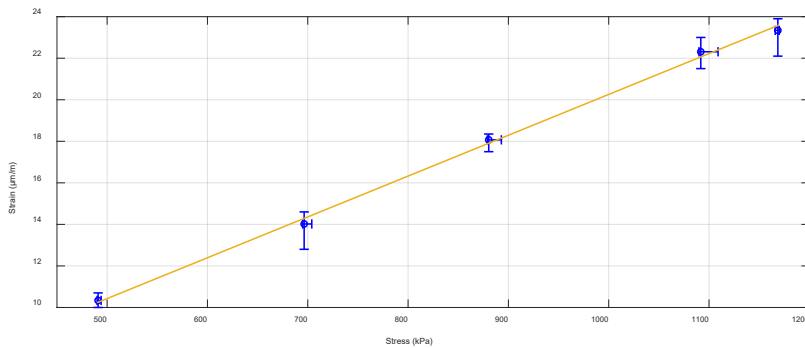


Fig. 3.10. Received average FBG optical strain sensor's strain values (µm/m) for every induced stress (kPa) level made by the FWD device.

Table 3.2 presents received strain measurement values generated by the FWD devices versus the road pavement layer temperature. FWD device is positioned right on the embedment position of the FBG strain and temperature sensors. FWD load drops load – fixed to 50 kN (pressure 707 kPa) for each drop. As can be seen in Table 3.2, with the temperature range of 1–1.5 °C, the received average relative strain value at the recycled layer is 2.5 times higher than at 24.8–25.1 °C. Such results can be explained by the effect of temperature on the different layers of the road structure. As environmental temperature decreases, so does the temperature of the road's layer

materials. With lower temperatures, for example, during wintertime, upper asphalt layers are becoming stiffer, thus induced strain by the FWD device (or any other transport traffic vehicle) is more freely carried over to deeper layers of the road – recycled layer. The results show that the impact of temperatures is essential and should be taken into consideration during measurements and calibration of sensors. As a result, calibration of the sensors should be made not only depending on load or stress, but also on the temperature.

Table 3.2

Received strain measurement values induced by the FWD devices versus ambient temperature

The temperature of the cement-treated RAP mixture layer during the experiments	1–1.5 (°C)	24.8–25.1 (°C)
$\Delta\varepsilon_{avg}$ ( $\mu\text{m/m}$ )	34.63	13.70
Coefficient of variation (%)	4.26	6.57

As experiments with FBG strain optical sensor and FWD device approved the stable and correct operation, the next research phase consists of transport traffic strain monitoring experiments.

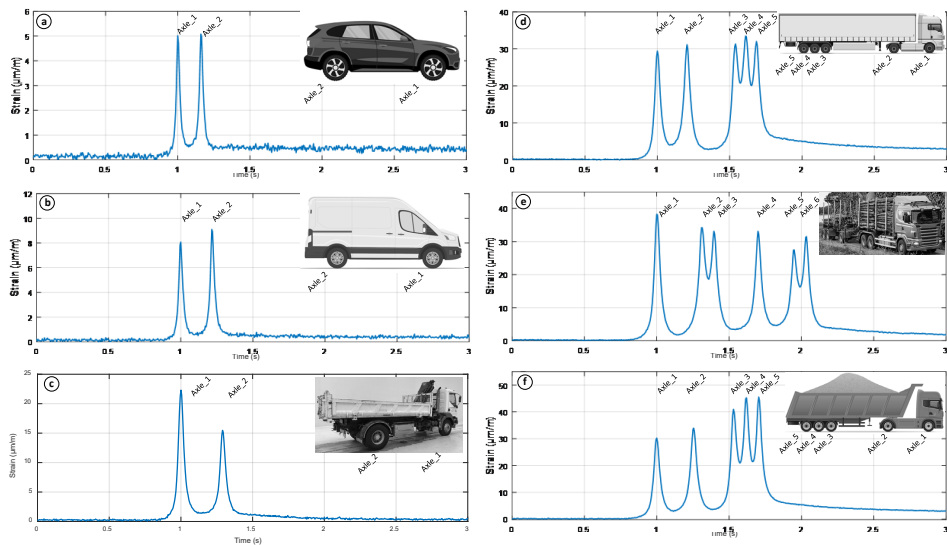


Fig. 3.11. Real-time traffic strain measurement data.

The temperature within the cement-treated RAP mixture layer, during experimental measurements, varies within a range of 1–1.5 °C. As there are different types of transportation passing the road, to better comprehend the strain-induced changes and their amount, we categorize all of the transport into 4 classes: 2 axle passenger cars (Fig. 3.11 (a)), 2 axle minibuses, vans (Fig. 3.11 (b)), 2–3 axle trucks (Fig. 3.11 (c)) and 4–6 axle trucks (Fig. 3.11 (d)–(f)).

Figure 3.11 presents measured strain-induced changes in time for 6 randomly chosen vehicles. As Fig. 3.11 shows, an embedded FBG optical strain sensor allows for precise detection of the strain-induced changes in time for each axle of a vehicle. The acquired results can be applied in determining the vehicle movement speed, e.g., the measurement in Fig. 3.11 (a) for a BMW X5 car (distance between axles 2.975 m) the measured time between strain peaks (axle points) is 0.164 ms. Based on this data, we can calculate that the movement speed of this car is 65.3 km/h.

It is essential to point out that depending on the vehicle type, mass, and number of axles, the strain value relaxation time is different. The typical recovery time for passenger cars is up to 3 sec, but for trucks – typically up to 5 sec.

Table 3.3 summarizes the data on strain value intervals (for a vehicle axle) for each group of vehicles. The strain intervals are divided into 2 types: 1) induced strain shift range; 2) typical (90 % events) strain shift range. The measurements show that passenger car axles typically induce 2–10 times less strain than the axles of 2 axle vans and 3–45 times less strain than 4–6 axle trucks.

Table 3.3

Measured induced strain shift range and calculated typical strain shift of real-time traffic

	 2 axle passenger car	 2 axle vans	 2–3 axle trucks	 4–6 axle trucks
<b>Induced strain shift range (<math>\mu\text{m}/\text{m}</math>)</b>	0.7–6	4.6–13	10–38	12–42
<b>Typical (90 % events) strain shift range (<math>\mu\text{m}/\text{m}</math>)</b>	0.8–4.1	5.5–8.5	11–26	14–36

### Summary

The research results allow concluding that embedded (anchor) type FBG sensors are the most appropriate for measuring road pavement strain caused by vehicles. For road monitoring purposes, FBG strain sensors should be calibrated not only depending on the applied load, but also on road layer temperature. High sensitivity of FBG sensors allows strain measuring for each vehicle axle. Experiments and measured results are very topical for local and international road pavement designers and road management services to forecast the potential collapse of the road, permanent deformation, weight of the vehicles and number of their axles, as well as for traffic monitoring, and road pavement temperature monitoring. These data also can be used for smart road solutions [97] for traffic flow analysis, vehicle counting, and free parking lots analysis.

The original publications on the research discussed in this subsection are attached (**Annexes VIII –XI** to the Thesis).

## CONCLUSIONS

1. The most valuable results (reflectivity = 90.3 %, FWHM = 0.112 nm, SLS = 35.6 dB) for long-distance monitoring solutions based on FBG sensors network were achieved using FBG with the raised sine apodization at  $\Delta n = 1 \times 10^{-4}$  and  $L = 20$  mm.
2. FBG sensors' network (40 sensors) with the raised sine apodization at  $\Delta n = 1 \times 10^{-4}$  and grating length of 20 mm can be used in 60 km and longer monitoring solutions.
3. For the hybrid single broadband light source-based system with 10 Gbit/s 32-channels SS-WDM PON and 5 FBG sensor network, the received BER is  $4 \times 10^{-7}$ , but for the system without an FBG network –  $2 \times 10^{-7}$ . The FBG sensor network had an insignificant impact on the data transmission system.
4. Power penalty for the SS-WDM data transmission and sensor system with and without an FBG sensor at FEC threshold of  $2.3 \times 10^{-3}$  without the transmission line is 0.5 dB, but with 20 km long SMF it is 0.2 dB.
5. Considering the experimental road measurement results, it can be stated that embedded (anchor) type FBG strain sensors are most suitable for embedment into the road pavement, allowing for real-time assessment of the strain induced by traffic loads and performing the structural health monitoring.
6. Axles of passenger cars normally cause 2–10 times less strain in the cement-treated RAP mixture layer compared to 2 axle vans (0.7–6  $\mu\text{m/m}$  and 4.6–13  $\mu\text{m/m}$ , respectively) and 3–45 times less strain than 4–6 axle trucks (12–42  $\mu\text{m/m}$ ).

The recommendations formulated during the development of the Thesis are intended for:

- FBG sensor network designers and manufacturers;
- optimization of the existing optical metro access networks in use, as well as establishment of the new ones;
- local and international road pavement designers and road maintenance service providers, developers and manufacturers of smart road solutions.

The results achieved during the Thesis development and reported in the research have been presented in 5 scientific articles, 4 scientific conference proceedings (indexed in Scopus, IEEE and Web of Science), one monograph, and one patent issued by the Republic of Latvia. The research results were also presented at 13 scientific conferences (proceedings not indexed in Scopus, IEEE, Web of Science).

Participation in public events: European Researchers' Night, Latvian Radio 1 podcast "Zināmais nezināmajā", RTU homepage, Magazine "IR", Delfi, LMT, LETA, IZM, labsoflatvia, *Dienas Bizness*, LA.lv, etc.

## REFERENCES

1. A. Abdelgawad and K. Yelamarthi, Internet of Things (IoT) platform for structure health monitoring, *Wireless Communications and Mobile Computing*, vol. 2017, Article ID 6560797, 10 pages, 2017. DOI: [doi.org/10.1155/2017/6560797](https://doi.org/10.1155/2017/6560797).
2. Q. Jin, Z. Liu, J. Bin, and W. Ren, Predictive analytics of in-service bridge structural performance from SHM data mining perspective: a case study, *Shock and Vibration*, vol. 2019, Article ID 6847053, 11 pages, 2019. DOI: [doi.org/10.1155/2019/6847053](https://doi.org/10.1155/2019/6847053).
3. H. Xu, F. Li, W. Zhao, S. Wang, Y. Du, and C. Bian, A high precision fiber Bragg grating inclination sensor for slope monitoring, *Journal of Sensors*, vol. 2019, Article ID 1354029, 7 pages, 2019. DOI: [doi.org/10.1155/2019/1354029](https://doi.org/10.1155/2019/1354029).
4. L. Fan, Y. Bao. Review of fiber optic sensors for corrosion monitoring in reinforced concrete. *Cem. Concr. Compos.* 2021, 120, 104029. DOI: [doi.org/10.1016/j.cemconcomp.2021.104029](https://doi.org/10.1016/j.cemconcomp.2021.104029).
5. D. Budnicki, I. Parola, Ł. Szostkiewicz, K. Markiewicz, Z. Hołdyński, G. Wojcik, M. Makara, K. Poturaj, M. Kuklińska, P. Mergo, et al. All-Fiber Vector Bending Sensor Based on a Multicore Fiber With Asymmetric Air-Hole Structure. *J. Light. Technol.* 2020, 38, 6685–6690. DOI: [doi.org/10.1109/JLT.2020.3012769](https://doi.org/10.1109/JLT.2020.3012769).
6. G. K. Ekechukwu, J. Sharma. Well-scale demonstration of distributed pressure sensing using fiber-optic DAS and DTS. *Sci. Rep.* 2021, 11, 12505. DOI: [doi.org/10.1038/s41598-021-91916-7](https://doi.org/10.1038/s41598-021-91916-7).
7. F. Lu, R. Wright, P. Lu, P. C. Cvetcic, P. R. Ohodnicki, Distributed fiber optic pH sensors using sol-gel silica based sensitive materials. *Sens. Actuators B Chem.* 2021, 340, 129853. DOI: [doi.org/10.1016/j.snb.2021.129853](https://doi.org/10.1016/j.snb.2021.129853).
8. Y. Liu, A. Zhou, L. Yuan, Multifunctional fiber-optic sensor, based on helix structure and fiber Bragg gratings, for shape sensing. *Opt. Laser Technol.* 2021, 143, 107327. DOI: [doi.org/10.1016/j.optlastec.2021.107327](https://doi.org/10.1016/j.optlastec.2021.107327).
9. U. Senkans, J. Braunfelds, I. Lyashuk, J. Porins, S. Spolitis, V. Bobrovs, Research on FBG-Based Sensor Networks and Their Coexistence with Fiber Optical Transmission Systems. *J. Sens.* 2019, 2019, 6459387. DOI: [doi.org/10.1155/2019/6459387](https://doi.org/10.1155/2019/6459387).
10. C. He, S. Korposh, R. Correia, L. Liu, B. R. Hayes-Gill, S. P. Morgan, Optical fibre sensor for simultaneous temperature and relative humidity measurement: Towards absolute humidity evaluation. *Sens. Actuators B Chem.* 2021, 344, 130154. DOI: [doi.org/10.1016/j.snb.2021.130154](https://doi.org/10.1016/j.snb.2021.130154).
11. J. Braunfelds, U. Senkans, P. Skels, R. Janeliukstis, T. Salgals, D. Redka, I. Lyashuk, J. Porins, S. Spolitis, V. Haritonovs, V. Bobrovs, FBG-Based Sensing for Structural Health Monitoring of Road Infrastructure (2021) *Journal of Sensors*, 2021, art. no. 8850368. DOI: [doi.org/10.1155/2021/8850368](https://doi.org/10.1155/2021/8850368).

12. Taylor & Francis Group, Optical Fiber Sensors – Advances Techniques and Applications, CRC Press, 2015, pp. 545. DOI: doi.org/10.1201/b18074.
13. Advantages of optical sensor | Disadvantages of optical sensor. Available online: <http://www.rfwireless-world.com/Terminology/Advantages-and-Disadvantages-of-Optical-Sensor.html> (accessed on December 5, 2022).
14. J. Braunfelds, S. Spolitis, L. Gegere, D. Pikulins, V. Stepanovs and A. Supe, Demonstration of Polarization Optical-Time-Domain Reflectometer for Monitoring of Optical Fiber Lines, 2022 Workshop on Microwave Theory and Techniques in Wireless Communications (MTTW), 2022, pp. 9–12, DOI: doi.org/10.1109/MTTW56973.2022.9942583.
15. Li, X. Yang, C. Yang, S. Li, G. Fiber-Optical Sensors: Basics and Applications in Multiphase Reactors. *Sensors* 2012, 12, 12519–12544. DOI: doi.org/10.3390/s120912519.
16. A. D. Kersey et al., Fiber grating sensors, *Journal of Lightwave Technology*, vol. 15, no. 8, pp. 1442–1463, 1997, DOI: doi.org/10.1109/50.618377.
17. G. Rajan, *Optical Fiber Sensors: Advanced Techniques and Applications*. (2015), ISBN 9781482228250.
18. K. O. Hill and G. Meltz, Fiber Bragg grating technology fundamentals and overview, *Journal of Lightwave Technology*, vol. 15, no. 8, pp. 1263–1276, 1997, DOI: doi.org/10.1109/50.618320.
19. M. Götten, S. Lochmann, A. Ahrens, E. Lindner, J. Vlekken and J. Van Roosbroeck, A CDM-WDM Interrogation Scheme for Massive Serial FBG Sensor Networks, *IEEE Sensors Journal*, vol. 22, no. 12, pp. 11290–11296, 2022, DOI: doi.org/10.1109/JSEN.2021.3070446.
20. A. Barrias, J. R. Casas, S. Villalba, A Review of Distributed Optical Fiber Sensors for Civil Engineering Applications. *Sensors* 2016, 16, 748. DOI: doi.org/10.3390/s16050748.
21. T. Wu, G. Liu, S. Fu, F. Xing, Recent Progress of Fiber-Optic Sensors for the Structural Health Monitoring of Civil Infrastructure. *Sensors* 2020, 20, 4517. DOI: doi.org/10.3390/s20164517.
22. X. W. Ye, Y. H. Su, J. P. Han, Structural Health Monitoring of Civil Infrastructure Using Optical Fiber Sensing Technology: A Comprehensive Review, *The Scientific World Journal*, vol. 2014, Article ID 652329, 11 pages, 2014. DOI: doi.org/10.1155/2014/652329.
23. J. Braunfelds, U. Senkans, P. Skels, R. Janeliukstis, J. Porins, S. Spolitis, V. Bobrovs, Road Pavement Structural Health Monitoring by Embedded Fiber Bragg Grating Based Optical Sensors *Sensors*, 2022, pp. 1–13. DOI: doi.org/10.3390/s22124581.
24. P. Kara De Maeijer, G. Luyckx, C. Vuye, E. Voet, W. Van den Bergh, S. Vanlanduit, J. Braspeninckx, N. Stevens, J. De Wolf, Fiber Optics Sensors in Asphalt Pavement: State-of-the-Art Review. *Infrastructures* 2019, 4, 36. DOI: doi.org/10.3390/infrastructures4020036.

25. B. Van Esbeen, C. Finet, R. Vandebrouck, D. Kinet, K. Boelen, C. Guyot, G. Kouroussis, C. Caucheteur, Smart Railway Traffic Monitoring Using Fiber Bragg Grating Strain Gauges. *Sensors* 2022, 22, 3429. DOI: doi.org/10.3390/s22093429.
26. S. Cocking, H. Alexakis, M. DeJong, (2021). Distributed dynamic fibre-optic strain monitoring of the behaviour of a skewed masonry arch railway bridge. *Journal of Civil Structural Health Monitoring*, 11 (4), 989–1012. DOI: doi.org/10.1007/s13349-021-00493-w.
27. G. Kouroussis, D. Kinet, V. Moeyaert, J. Dupuy, C. Caucheteur, (2016). Railway structure monitoring solutions using fibre Bragg grating sensors. *International Journal of Rail Transportation*, 4(3), 135–150. DOI: doi.org/10.1080/23248378.2016.1184598.
28. K. Čápková, L. Velebil, J. Včelák, M. Dvořák, L. Šašek, (2019). Environmental Testing of a FBG Sensor System for Structural Health Monitoring of Building and Transport Structures. *Procedia Structural Integrity*, 17, 726–733. DOI: doi.org/10.1016/j.prostr.2019.08.097.
29. C. Li, J. Tang, C. Cheng, L. Cai, M. Yang, FBG Arrays for Quasi-Distributed Sensing: A Review. *Photonic Sensors*, 11(1), 91–108, 2021. DOI: doi.org/10.1007/s13320-021-0615-8.
30. S.-F. Jiang, Z.-H. Qiao, N.-L. Li, J.-B. Luo, S. Shen, M.-H. Wu, Y. Zhang, Structural Health Monitoring System Based on FBG Sensing Technique for Chinese Ancient Timber Buildings. *Sensors*, 20(1), 2019, 110. DOI: doi.org/10.3390/s20010110.
31. A. Kefal, I. E. Tabrizi, M. Tansan, E. Kisa, M. Yildiz, An experimental implementation of inverse finite element method for real-time shape and strain sensing of composite and sandwich structures. *Composite Structures*, 258, 113431, 2021. DOI: doi.org/10.1016/j.compstruct.2020.1131.
32. Y. Zhan, F. Lin, Z. Song, Z. Sun, M. Yu, Applications and research progress of optical fiber grating sensing in thermoplastic composites molding and structure health monitoring. *Optik*, 229, 166122, 2021. DOI: doi.org/10.1016/j.ijleo.2020.166122.
33. R. Di Sante, Fibre Optic Sensors for Structural Health Monitoring of Aircraft Composite Structures: Recent Advances and Applications. *Sensors*, 15(8), 18666–18713, 2021. DOI: doi.org/10.3390/s150818666.
34. C. Campanella, A. Cuccovillo, C. Campanella, A. Yurt, V. Passaro, (2018). Fibre Bragg Grating Based Strain Sensors: Review of Technology and Applications. *Sensors*, 18(9), 3115. DOI: doi.org/10.3390/s18093115.
35. D. Lo Presti et al., Wearable System Based on Flexible FBG for Respiratory and Cardiac Monitoring, *IEEE Sensors Journal*, vol. 19, no. 17, pp. 7391–7398, 2019, DOI: doi.org/10.1109/JSEN.2019.2916320.
36. D. Lo Presti et al., Fiber Bragg Gratings for Medical Applications and Future Challenges: A Review, *IEEE Access*, vol. 8, pp. 156863–156888, 2020, DOI: 10.1109/ACCESS.2020.3019138.

37. A. Mendez, Fiber Bragg grating sensors for biomedical applications, *Photonics and Fiber Technology 2016* (ACOFT, BGPP, NP), OSA Technical Digest (online) (Optica Publishing Group, 2016), paper BM4B.1. DOI: doi.org/10.1364/BGPP.2016.BM4B.1.
38. Q. Liu, Z. L. Ran, Y. J. Rao, S. C. Luo, H. Q. Yang and Y. Huang, Highly Integrated FP/FBG Sensor for Simultaneous Measurement of High Temperature and Strain, *IEEE Photonics Technology Letters*, vol. 26, no. 17, pp. 1715-1717, 2014, DOI: doi.org/10.1109/LPT.2014.2331359.
39. S. Ma, Y. Xu, Y. Pang, X. Zhao, Y. Li, Z. Qin, Z. Liu, P. Lu, X. Bao, Optical Fiber Sensors for High-Temperature Monitoring: A Review. *Sensors* 2022, 22, 5722. DOI: doi.org/10.3390/s22155722.
40. C. Dutta, J. Kumar, T. K. Das and S. P. Sagar, Recent Advancements in the Development of Sensors for the Structural Health Monitoring (SHM) at High-Temperature Environment: A Review, *IEEE Sensors Journal*, vol. 21, no. 14, pp. 15904–15916, 2021, DOI: doi.org/10.1109/JSEN.2021.3075535.
41. J. Juraszek, P. Antonik-Popiołek, Fibre Optic FBG Sensors for Monitoring of the Temperature of the Building Envelope. *Materials* (Basel). 2021 ;14(5):1207. DOI: 10.3390/ma14051207.
42. Q. Wang, L. Zhang, C. Sun, and Q. Yu, Multiplexed Fiber-Optic Pressure and Temperature Sensor System for Down-Hole Measurement, *IEEE Sensors Journal*, vol. 8, no. 11, pp. 1879–1883, 2008, DOI: doi.org/10.1109/JSEN.2008.2006253.
43. T. Li, J. Guo, Y. Tan, and Z. Zhou, Recent Advances and Tendency in Fiber Bragg Grating-Based Vibration Sensor: A Review, *IEEE Sensors Journal*, vol. 20, no. 20, pp. 12074–12087, 2020, DOI: doi.org/10.1109/JSEN.2020.3000257.
44. Y. Zhang, Z. Yin, B. Chen, H.-L. Cui, J. Ning, A novel fiber Bragg grating based seismic geophone for oil/gas prospecting, *Proc. SPIE*, vol. 5765, pp. 1112–1121, May 2005. DOI: doi.org/10.1117/12.599797.
45. P. Munendhar, S. K. Khijwania. Two-dimensional fiber Bragg grating based vibration sensor for structural health monitoring, *AIP Conference Proceedings* 1536, 1324–1326 (2013). DOI: doi.org/10.1063/1.4810731.
46. T. Li, C. Shi, Y. Tan, R. Li, Z. Zhou, and H. Ren, A Diaphragm Type Fiber Bragg Grating Vibration Sensor Based on Transverse Property of Optical Fiber with Temperature Compensation, *IEEE Sensors Journal*, vol. 17, no. 4, pp. 1021–1029, 2017, DOI: doi.org/10.1109/JSEN.2016.2641931.
47. T. Li, Y. Tan, Z. Zhou, (2017). String-type based two-dimensional fiber Bragg grating vibration sensing principle and structure optimization. *Sensors and Actuators A: Physical*, 259, 85–95. DOI:10.1016/j.sna.2017.03.031.

48. L. Wei, L. Yu, J. Wang, D. Jiang, Q. Liu and Z. Liu, An FBG-Sensing Two-Dimensional Vibration Sensor Based on Multi-Axis Flexure Hinge, *IEEE Sensors Journal*, vol. 19, no. 10, pp. 3698–3710, 2019, DOI: [doi.org/10.1109/JSEN.2019.2895232](https://doi.org/10.1109/JSEN.2019.2895232).
49. Z. M. Hafizi, E. Vorathin, A Temperature-Compensated FBG Pressure Sensor for Underwater Pipeline Monitoring, 2020 IEEE 8th International Conference on Photonics (ICP), 2020, pp. 66–67, DOI: [doi.org/10.1109/ICP46580.2020.9206469](https://doi.org/10.1109/ICP46580.2020.9206469).
50. J. Wang, L. Zhao, T. Liu, Z. Li, T. Sun, K. T. V. Grattan, Novel Negative Pressure Wave-Based Pipeline Leak Detection System Using Fiber Bragg Grating-Based Pressure Sensors, *Journal of Lightwave Technology*, vol. 35, no. 16, pp. 3366–3373, 2017, DOI: [doi.org/10.1109/JLT.2016.2615468](https://doi.org/10.1109/JLT.2016.2615468).
51. P.-L. Ko, K.-C. Chuang, C.-C. Ma, A Fiber Bragg Grating-Based Thin-Film Sensor for Measuring Dynamic Water Pressure, *IEEE Sensors Journal*, vol. 18, no. 18, pp. 7383–7391, 2018, DOI: [doi.org/10.1109/JSEN.2018.2857561](https://doi.org/10.1109/JSEN.2018.2857561).
52. L. Xiong, Y. Guo, W. Zhou, M. Chen and X. Zhou, Fiber Bragg Grating-Based Three-Axis Vibration Sensor, *IEEE Sensors Journal*, vol. 21, no. 22, pp. 25749–25757, 2021, DOI: [doi.org/10.1109/JSEN.2021.3118360](https://doi.org/10.1109/JSEN.2021.3118360).
53. X. Li et al., An FBG Pressure Sensor Based on Spring-Diaphragm Elastic Structure for Ultimate Pressure Detection, *IEEE Sensors Journal*, vol. 22, no. 3, pp. 2213–2220, 2022, DOI: [doi.org/10.1109/JSEN.2021.3136212](https://doi.org/10.1109/JSEN.2021.3136212).
54. M. Liu, Y. Wu, C. Du, D. Jiang, Z. Wang, FBG-Based Liquid Pressure Sensor for Distributed Measurement with a Single Channel in Liquid Environment, *IEEE Sensors Journal*, vol. 20, no. 16, pp. 9155–9161, 2020, DOI: [doi.org/10.1109/JSEN.2020.2986550](https://doi.org/10.1109/JSEN.2020.2986550).
55. L. Xiong, Y. Guo, G. Jiang, L. Jiang, X. Zhou, (2019). Fiber Bragg grating displacement sensor with high measurement accuracy for crack monitoring. *IEEE Sensors Journal*, 1–1. DOI: [doi.org/10.1109/jsen.2019.2930761](https://doi.org/10.1109/jsen.2019.2930761).
56. Y. Chen, J. Wu, X. Zhao, Monitoring of vertical displacement of concrete slab end at pavement joint based on FBG-dowel bar signal. *J. Transp. Eng. B Pavements* 2022, 148, 04022012. DOI: [doi.org/10.1061/JPEODX.0000358](https://doi.org/10.1061/JPEODX.0000358).
57. M. Bonopera, Fiber-Bragg-Grating-Based Displacement Sensors: Review of Recent Advances. *Materials (Basel)*. 2022; 15(16):5561. DOI: [doi.org/10.3390/ma15165561](https://doi.org/10.3390/ma15165561).
58. C. Hong, Y. Zhang, Y. Yang, Y. Yuan, A FBG based displacement transducer for small soil deformation measurement. *Sensors and Actuators A: Physical*, 286, 35–42, 2019. DOI: [doi.org/10.1016/j.sna.2018.12.022](https://doi.org/10.1016/j.sna.2018.12.022).
59. J. Thomas, T. R. Rajanna, S. Asokan, Temperature compensated FBG displacement sensor for long-range applications. *IEEE Sens. Lett.* 2020, 4, 8931563. DOI: [doi.org/10.1109/LESENS.2019.2959377](https://doi.org/10.1109/LESENS.2019.2959377).

60. Z. Lu, C. Hong, Y. Zhang, D. Su and Y. Fu, Development of an FBG Sensor for Measuring Large Range and Multi-Directional Settlement, *IEEE Access*, vol. 7, pp. 107669–107677, 2019, DOI: doi.org/10.1109/ACCESS.2019.2932774.
61. H. Li, G. Xu, X. Gui, L. Liang, Z. Li, An FBG Displacement Sensor in Deformation Monitoring of Subway Floating Slab. *IEEE Sensors Journal*, 21(3), 2963–2971, 2021. DOI: doi.org/10.1109/jsen.2020.3022466.
62. G. Lyu, C. Bi, Y. Zhang, C. Wang, M. Wang, X. Jiang, Large-range bridge beam-gap displacement sensors based on cantilever beam with fiber Bragg grating. *Lect. Notes Electr. Eng.* 2020, 567, 3–11. DOI: doi.org/10.1007/978-981-13-8595-7\_1.
63. C. Li, L. Sun, Z. Xu, X. Wu, T. Liang, W. Shi. Experimental Investigation and Error Analysis of High Precision FBG Displacement Sensor for Structural Health Monitoring. *International Journal of Structural Stability and Dynamics*, 2020. DOI: doi.org/10.1142/s0219455420400118.
64. M. Bonopera, K. C. Chang, C. C. Chen, Z. K. Lee, Y. C. Sung, N. Tullini, Fiber Bragg grating–differential settlement measurement system for bridge displacement monitoring: Case study. *J. Bridge Eng.* 2019, 24, 05019011. DOI: doi.org/10.1061/(asce)be.1943-5592.0001470.
65. M. A. Alias, M. F. Ismail, M. S. M. Sa’ad, et al., A high-precision extensometer system for ground displacement measurement using fiber Bragg grating. *IEEE Sens. J.* 2022, 22, 8509–8521. DOI: doi.org/10.1109/jsen.2022.3159850.
66. M. Maheshwari, Y. Yang, D. Upadrashta and T. Chaturvedi, A Rotation Independent In-Place Inclinometer/Tilt Sensor Based on Fiber Bragg Grating, *IEEE Transactions on Instrumentation and Measurement*, vol. 68, no. 8, pp. 2943–2953, Aug. 2019, DOI: doi.org/10.1109/TIM.2018.2870246.
67. HBM, Optical Fiber Sensors, Available online: [https://www.hbm.com/en/4599/new-light-optical-fiber-sensors/?product\\_type\\_no=newLight](https://www.hbm.com/en/4599/new-light-optical-fiber-sensors/?product_type_no=newLight) (accessed on December 11, 2022).
68. Smart fibres, FBG sensors, Available online: <https://www.smartfibres.com/products> (accessed on December 11, 2022).
69. Sylex, ES-03 Embeddable strain sensor, p. 2. 2021.
70. K. M. Dwivedi, G. Trivedi and S. K. Khijwania, Theoretical Study and Optimization of Apodized Fiber Bragg Grating for Single and Quasi-distributed Structural Health Monitoring Applications, 2020, 30th International Conference Radioelektronika (RADIOELEKTRONIKA), 2020, pp. 1–6, DOI: doi.org/10.1109/RADIOELEKTRONIKA49387.2020.9092399.
71. A. Rumadi, D. Syahriar, Astharini, and A. H. Lubis, The effects of apodization profile on uniform fiber Bragg gratings, 2015 9th International Conference on Telecommunication

- Systems Services and Applications (TSSA), 2015, pp. 1–6, DOI: doi.org/10.1109/TSSA.2015.7440430.
72. I. Ashry, A. Elrashidi, A. Mahros, M. Alhaddad, and K. Elleithy, Investigating the performance of apodized Fiber Bragg gratings for sensing applications, *Proceedings of the 2014 Zone 1 Conference of the American Society for Engineering Education*, 2014, pp. 1–5, DOI: doi.org/10.1109/ASEEZone1.2014.6820640.
  73. Optiwave, Photonic Software, OptiGrating, Available online: <https://optiwave.com/products/component-design/optigrating/optigrating/> (accessed on December 11, 2022).
  74. Optiwave, OptiGrating User's Reference and Tutorials, p. 214, 2008.
  75. Z. A. El-Sahn, W. Mathlouthi, H. Fathallah, S. LaRochelle, and L. A. Rusch, Dense SS-WDM over legacy PONs: smooth upgrade of existing FTTH networks, *Journal of Lightwave Technology*, vol. 28, no. 10, pp. 1485–1495, 2010. DOI: doi.org/10.1109/jlt.2010.2046313.
  76. ITU-T, Spectral grids for WDM applications: DWDM frequency grid (G.694.1), 2020, p. 16.
  77. Technica, T840 / Rugged In-Line Temperature Sensor, 2022, p. 2.
  78. W. Tsai et al. A 20-m/40-Gb/s 1550-nm DFB LD-Based FSO Link, *IEEE Photonics J.*, 2015, 7, 1–7, DOI: doi.org/10.1109/JPHOT.2015.2506172.
  79. Jr. N. Ledentsov, M. Agustin, L. Chorchos, et al., Energy efficient 850-nm VCSEL based optical transmitter and receiver link capable of 56 Gbit/s NRZ operation, *Vertical-Cavity Surface-Emitting Lasers XXIII*, 109380J, 2019, pp. 1–8. DOI: doi.org/10.1117/12.2509916.
  80. K. Elayoubi, A. Rissons, A. Belmonte, Optical test bench experiments for 1-Tb/s satellite feeder uplinks, *Laser Communication and Propagation through the Atmosphere and Oceans VII*, 1077006, 2018, pp. 1–11. DOI: doi.org/10.1117/12.2317728.
  81. X. Ma, T. Wang, Z. Dong, Dynamic Response Monitoring and Analysis of In-Service Asphalt Pavement Based on FBG Measuring Technology. In: Chabot, A., Hornych, P., Harvey, J., Loria-Salazar, L. (eds) *Accelerated Pavement Testing to Transport Infrastructure Innovation. Lecture Notes in Civil Engineering*, vol 96. Springer, Cham, 2020. DOI: doi.org/10.1007/978-3-030-55236-7\_55
  82. J. Braunfelds, U. Senkans, P. Skels, I. Murans, J. Porins, S. Spolitis, V. Bobrovs, Fiber Bragg Grating Optical Sensors for Road Infrastructure Monitoring Applications, (2022) *Optics InfoBase Conference Papers, Applied Industrial Optics*, pp. 1–2, DOI: doi.org/10.1364/AIO.2022.W1A.2.
  83. W. Liu, X. Liu, Z. Wang, Z. Zhi, High temperature deformation investigation of asphalt mixture with nanosized volcanic ash fillers using optical fiber sensor. *Measurement* 2019, 140, 171–181. DOI: doi.org/10.1016/j.measurement.2019.03.075.

84. J. Xie, H. Li, L. Gao, M. Liu, Laboratory investigation of rutting performance for multilayer pavement with fiber Bragg gratings. *Constr. Build. Mater.* 2017, 154, 331–339. DOI: doi.org/10.1016/j.conbuildmat.2017.07.233.
85. S.-Z. Chen, G. Wu, D.-C. Feng, L. Zhang, Development of a bridge weigh-in-motion system based on long-gauge fiber Bragg grating sensors. *J. Bridge Eng.* 2018, 23, 04018063. DOI: doi.org/10.1061/(asce)be.1943-5592.0001283.
86. M. Al-Tarawneh, Y. Huang, P. Lu and R. Bridgelall, Weigh-In-Motion System in Flexible Pavements Using Fiber Bragg Grating Sensors Part A: Concept, *IEEE Transactions on Intelligent Transportation Systems*, vol. 21, no. 12, pp. 5136–5147, 2020, doi: 10.1109/TITS.2019.2949242.
87. K. Yuksel, D. Kinet, K. Chah, C. Caucheteur, Implementation of a Mobile Platform Based on Fiber Bragg Grating Sensors for Automotive Traffic Monitoring. *Sensors* 2020, 20, 1567. DOI: doi.org/10.3390/s20061567.
88. Anritsu corporation, MS9740A Optical Spectrum Analyzer Operation Manual, 23rd Edition, p. 320.
89. Safibra: Composite sensor. Available online: <http://www.safibra.cz/en/composite-sensor> (accessed on December 5, 2022).
90. Safibra: FBG temperature sensor. Available online: <http://www.safibra.cz/en/fbg-temperature-sensor> (accessed on December 5, 2022).
91. P. Ullidtz, *Modelling Flexible Pavement Response and Performance*, Polyteknisk Forlag, Denmark, ISBN: 8750208055, 1998.
92. L. Korkiala-Tanttu, *Calculation Method for Permanent Deformation of Unbound Pavement Materials*, VTT Technical Research Centre of Finland, Espoo, Finland, 2008.
93. T. Saevarsdottir and S. Erlingsson, Deformation modelling of instrumented flexible pavement structure, *Procedia Engineering*, vol. 143, pp. 937–944, 2016. DOI: doi.org/10.1016/j.proeng.2016.06.076.
94. P. Kara De Maeijer, W. Van den Bergh, and C. Vuye, Fiber Bragg Grating Sensors in Three Asphalt Pavement Layers, *Infrastructures*, vol. 3, 16, 2018. DOI: doi.org/10.3390/infrastructures3020016.
95. ES-01 Embeddable strain sensor. Available online: <https://www.sylex.sk/wp-content/uploads/2018/09/ES-01-Embeddable-strain-sensor.pdf> (24.05.2022.).
96. Xi'an Aurora Technology, Fiber Bragg Grating Embedded FBG Temperature Sensor, 2022.
97. Intel: Smart Roads Start with Smart Infrastructure, Available online: <https://www.intel.com/content/www/us/en/transportation/smart-road-infrastructure.html> (accessed on January 3, 2023).



**Jānis Braunfelds** was born in 1994 in Talsi. He obtained a Bachelor degree of Engineering Science in Electrical Science (2016) and a Master degree of Engineering Science in Telecommunications (2018) from Riga Technical University. Since 2016 he has been a research assistant with RTU. Currently, he is a researcher and lecturer at RTU. Since 2019, he has been a member of the RTU ETF Council, since 2021, a member of RTU Council of Science, and since 2022, a member of the RTU Council. He has been an international student in the Technical University of Eindhoven (TU/e) and the Technical University of Denmark. He is the owner of the following awards: the annual Award in Education and Science of Latvian Federation of Security and Defense Industries (2019), the Award of the Young Scientist of the Year 2020 of Latvian Student Association, and RTU Student Award in Valorisation 2020.